Physics Letters B 783 (2018) 95–113

Contents lists available at ScienceDirect

Physics Letters B

www.elsevier.com/locate/physletb

Constraints on jet quenching in p–Pb collisions at $\sqrt{s_{\rm NN}} = 5.02$ TeV measured by the event-activity dependence of semi-inclusive hadron-jet distributions

ALICE Collaboration *

ARTICLE INFO

Article history:
Received 19 December 2017
Received in revised form 12 March 2018
Accepted 22 May 2018
Available online 24 May 2018
Editor: M. Doser

ABSTRACT

The ALICE Collaboration reports the measurement of semi-inclusive distributions of charged-particle jets recoiling from a high-transverse momentum trigger hadron in p–Pb collisions at $\sqrt{s_{\rm NN}} = 5.02$ TeV. Jets are reconstructed from charged-particle tracks using the anti-$k_{\rm T}$ algorithm with resolution parameter $R = 0.2$ and 0.4. A data-driven statistical approach is used to correct the uncorrelated background jet yield. Recoil jet distributions are reported for jet transverse momentum $15 < p_{\rm T,jet}^{\rm ch} < 50$ GeV/c and are compared in various intervals of p–Pb event activity, based on charged-particle multiplicity and zero-degree neutral energy in the forward (Pb-going) direction. The semi-inclusive observable is self-normalized and such comparisons do not require the interpretation of p–Pb event activity in terms of collision geometry, in contrast to inclusive jet observables. These measurements provide new constraints on the magnitude of jet quenching in small systems at the LHC. In p–Pb collisions with high event activity, the average medium-induced out-of-cone energy transport for jets with $R = 0.4$ and $15 < p_{\rm T,jet}^{\rm ch} < 50$ GeV/c is measured to be less than 0.4 GeV/c at 90% confidence, which is over an order of magnitude smaller than a similar measurement for central Pb–Pb collisions at $\sqrt{s_{\rm NN}} = 2.76$ TeV. Comparison is made to theoretical calculations of jet quenching in small systems, and to inclusive jet measurements in p–Pb collisions selected by event activity at the LHC and in d–Au collisions at RHIC.

© 2018 European Organization for Nuclear Research. Published by Elsevier B.V. This is an open access article under the CC BY license (http://creativecommons.org/licenses/by/4.0/). Funded by SCOAP[3].

1. Introduction

The collision of heavy nuclei at high energies generates a Quark–Gluon Plasma (QGP), a dense, highly inviscid, strongly-coupled fluid governed by sub-nucleonic degrees of freedom [1]. While the structure and dynamical behavior of the QGP arise at the microscopic level from the interactions between quarks and gluons that are described by Quantum Chromodynamics (QCD), the QGP also exhibits emergent collective behavior. Current understanding of the properties of the QGP is based primarily on two phenomena observed in high energy nuclear collisions and their comparison to theoretical calculations: strong collective flow [2], and jet quenching, which arises from interaction of energetic jets with the medium [3].

Jets in hadronic collisions are generated by hard (high momentum transfer Q^2) interactions between quarks and gluons from the projectiles, with outgoing quarks and gluons from the interaction observed in detectors as correlated sprays of hadrons ("jets"). Theoretical calculations of jet production based on perturbative QCD (pQCD) are in excellent agreement over a broad kinematic range with jet measurements in pp collisions at the Large Hadron Collider (LHC) [4–7]. Measurements in pp collisions of charged-particle jets, which consist of the charged component of the hadronic jet shower, are also well-described by QCD-based Monte Carlo calculations [8,9].

In nuclear collisions, the interaction of jets with the QGP is expected to modify the observed rate of jet production and internal jet structure. Indeed, marked effects due to jet quenching have been observed for high transverse momentum (high-$p_{\rm T}$) hadrons and jets in central Au–Au collisions at the Relativistic Heavy Ion Collider (RHIC) [10–20] and in central Pb–Pb collisions at the LHC [9,21–32]. Jets therefore provide well-calibrated probes of the QGP.

Measurements of asymmetric p–Pb collisions at the LHC and of light nucleus–Au collisions at RHIC reveal evidence of collective effects that are similar in magnitude to those observed in symmetric collisions of heavy nuclei [33–50]. These measurements in asymmetric systems are reproduced both by model calculations that incorporate a locally thermalized hydrodynamic medium in the final state, and by calculations without QGP but with large fluctuations in the initial-state wavefunctions of the projectiles (see

* *E-mail address:* alice-publications@cern.ch.

https://doi.org/10.1016/j.physletb.2018.05.059
0370-2693/© 2018 European Organization for Nuclear Research. Published by Elsevier B.V. This is an open access article under the CC BY license (http://creativecommons.org/licenses/by/4.0/). Funded by SCOAP[3].

[51] and references therein). This raises the question whether a QGP is in fact generated in such light asymmetric systems, which were initially thought to be too small for the formation of a quasi-equilibrated fireball of matter in the final state [51]. Additional measurements, in particular to explore jet quenching in p–A collisions, will help to resolve this picture and to clarify the nature of equilibration in strongly-interacting matter.

There are several theoretical calculations currently available of jet quenching effects in p–Pb collisions at the LHC, which differ in their predictions. The calculation in [52] estimates the size of the region of high energy density to have a radius that is a factor 2 smaller in p–Pb than in central Pb–Pb collisions, with jet transport parameter $\hat{q}$, assumed to be proportional to charged multiplicity, to be a factor 7 smaller. Jet energy loss, which is proportional to $\hat{q}$ and depends on path length of the jet in the medium, is consequently expected in this calculation to be much smaller in p–Pb than in central Pb–Pb collisions. In contrast, a model calculation based on one-dimensional Bjorken hydrodynamics predicts large initial energy density in high multiplicity pp and p–Pb collisions [53]; this energy density corresponds to jet energy loss of several GeV, which is similar in magnitude to jet energy loss measured in central Pb–Pb collisions [9]. A calculation based on pQCD at next-to-leading order (NLO) finds negligible jet quenching effects for inclusive jet production in p–Pb collisions at $\sqrt{s_{\rm NN}} = 5$ TeV [54]. Finally, a QCD calculation of initial-state energy loss in cold nuclear matter (CNM) finds significant suppression of inclusive jet production for small-impact parameter p–Pb collisions at $\sqrt{s_{\rm NN}} = 5$ TeV [55].

Experimental searches for jet quenching effects in d–Au collisions at RHIC and in p–Pb collisions at the LHC have been carried out with high-$p_{\rm T}$ hadrons and reconstructed jets. These studies utilize both Minimum Bias (MB) events and more-differential event selection, in which events are characterized in terms of "event activity" (EA) based on central charged-particle multiplicity (ALICE [56]); forward charged-particle multiplicity (STAR [57], PHENIX [58,59], ALICE [56]); forward transverse energy (ATLAS [60], CMS [61]); or zero-degree neutral energy (STAR [57], ALICE [56]); where "forward" and "zero-degree" refer to the direction of the heavy nuclear projectile.

Inclusive hadron measurements in d–Au collisions at RHIC [57,58] exhibit yield enhancement in the region $2 < p_{\rm T} < 5\,{\rm GeV}/c$, which is commonly attributed to multiple scattering in the initial state, with no significant yield modification at higher $p_{\rm T}$ and with no significant difference observed between the MB and EA-selected distributions. For inclusive hadron measurements in p–Pb collisions at the LHC, ALICE does not observe significant yield modification for $p_{\rm T} > 8$ GeV/c in both MB and EA-selected events [56,62] while ATLAS and CMS observe yield enhancement for $p_{\rm T}$ greater than ~ 30 GeV/c in MB events [60,63,64], and ATLAS observes additional dependence on EA [60].

For inclusive jet production, no significant yield modification has been observed in MB p–Pb collisions at the LHC and MB d–Au collisions at RHIC [59,65–67]. However, measurements by the PHENIX collaboration at RHIC [59] and the ATLAS collaboration at the LHC [66] find apparent enhancement of the inclusive jet yield in EA-selected event populations thought to be biased towards large impact parameter in such asymmetric systems ("peripheral collisions"), with compensating suppression for event populations assigned small impact parameter ("central collisions"), while the ALICE collaboration finds no such yield modification as a function of event "centrality" [68].

Measurement of jet quenching effects with inclusive processes requires scaling of the inclusive yield from a reference collision system (usually pp) by the nuclear overlap function $\langle T_{\rm aA} \rangle$, with the angle brackets $\langle \ldots \rangle$ indicating an average over the event population; for current measurements, "aA" denotes d–Au at RHIC and p–Pb at the LHC. For an EA-selected population, $\langle T_{\rm aA} \rangle$ is calculated by correlating EA with collision geometry and applying Glauber modeling [69]. However, the correlation of EA with collision geometry in p–Pb collisions is obscured by large fluctuations in the EA observables [56], and can be biased by conservation laws and by dynamical correlations when measuring high Q^2 processes [70–75]. Color fluctuations in the proton wavefunction may induce a bias in soft particle production for p–Pb events tagged by a hard process, thereby biasing the correlation between EA and collision geometry [76–79]. A model calculation shows that selection bias can modify the scaling factor for jet production in peripheral $A+A$ relative to pp collisions, generating an apparent suppression of jet production in peripheral $A+A$ collisions if the Glauber calculation does not take this effect into account [80]; similar considerations apply to asymmetric collision systems.

While Glauber modeling for peripheral d–Au collisions at RHIC has been validated experimentally for moderate Q^2 processes using a proton-stripping process and knowledge of the deuteron wavefunction [57], no such check is possible with the proton beam at the LHC. It is therefore crucial to measure the EA-dependence of jet quenching effects in p–Pb collisions at the LHC with correlation observables that do not require the interpretation of EA in terms of collision geometry.

A correlation measurement of dijet transverse-momentum balance in p–Pb collisions at $\sqrt{s_{\rm NN}} = 5.02$ TeV finds no significant difference from a simulated pp reference distribution, independent of EA [61]. Measurements of dijet acoplanarity, which can be generated by both initial-state and final-state effects, likewise find no significant modification due to nuclear matter effects in EA-selected p–Pb collisions at $\sqrt{s_{\rm NN}} = 5.02$ TeV, relative to simulated distributions for pp collisions [61,81]. While these measurements provide qualitative indications, based on comparison to simulations, that final-state jet quenching effects in high-EA p–Pb collisions are small, quantitative measurements or limits on jet quenching effects in such collisions are still lacking.

In this paper we present measurements sensitive to jet quenching in p–Pb collisions at $\sqrt{s_{\rm NN}} = 5.02$ TeV, based on the semi-inclusive distribution of charged jets recoiling from a high-$p_{\rm T}$ trigger hadron [82]. The observable used in this analysis has been measured in pp collisions at $\sqrt{s} = 7$ TeV and compared to calculations based on PYTHIA and on pQCD at NLO, with PYTHIA providing a better description [9]. It has also been used to measure jet quenching effects in Pb–Pb collisions at $\sqrt{s_{\rm NN}} = 2.76$ TeV [9] and in Au–Au collisions at $\sqrt{s_{\rm NN}} = 200$ GeV [20].

The semi-inclusive recoil jet distribution is equivalent to the ratio of inclusive cross sections [9]; comparison of such self-normalized coincidence distributions for p–Pb event populations with different EA therefore does not require scaling by the nuclear overlap function $\langle T_{\rm pPb} \rangle$. Measurement of this observable in p–Pb collisions is sensitive to jet quenching effects, and indeed does not require interpretation of the EA in terms of p–Pb collision geometry. This approach thereby avoids potential bias due to Glauber modeling when interpreting the measurement.

We report charged recoil jet distributions reconstructed with the anti-$k_{\rm T}$ algorithm [83] in the range $15 < p_{\rm T,jet}^{\rm ch} < 50\,{\rm GeV}/c$, for jet resolution parameters $R = 0.2$ and 0.4. Correction of the jet yield for background uncorrelated with the triggered hard process, including multi-partonic interactions (MPI), is carried out statistically at the level of ensemble-averaged distributions, using the data-driven method first applied in [9]. EA in p–Pb collisions is characterized by two different observables, forward charged-particle multiplicity and neutral energy along the beam axis, both measured in the direction of the Pb-beam [56]. Jet quenching effects are quantified by comparing the measured distributions in

different EA classes of the p–Pb dataset. The results are compared to other jet quenching measurements and to theoretical calculations of jet quenching in asymmetric collision systems.

The paper is organized as follows: Sect. 2 describes the data set and analysis; Sect. 3 describes event selection based on trigger hadrons and event activity; Sect. 4 describes jet reconstruction; Sect. 5 discusses the semi-inclusive observable and presents the raw data; Sect. 6 discusses corrections; Sect. 7 discusses systematic uncertainties; Sect. 8 presents results and discussion; Sect. 9 compares the results to other measurements; and Sect. 10 is the summary.

2. Data set and analysis

The ALICE detector and performance are described in [84,85]. The data used in this analysis were recorded during the 2013 LHC run with p–Pb collisions at $\sqrt{s_{\rm NN}} = 5.02$ TeV. The Pb-going direction has rapidity $y > 0$ and pseudorapidity $\eta > 0$ in the laboratory frame. The per-nucleon momenta of the beams in this run were imbalanced in the laboratory frame, with the nucleon–nucleon center-of-mass at rapidity $y_{\rm NN} = -0.465$. The acceptance of tracks and jets in this analysis are specified in terms of $y^* = y_{\rm LAB} - y_{\rm NN}$, where $y_{\rm LAB}$ denotes the rapidity measured in the laboratory frame.

Events were selected online by an MB trigger, which requires the coincidence of signals in the V0A and V0C forward scintillator arrays. The V0A array has acceptance $2.8 < \eta < 5.1$ and the V0C array has acceptance $-3.7 < \eta < -1.7$, both covering the full azimuth. Offline event selection also utilizes the Zero-Degree Calorimeters (ZDC), which are neutron calorimeters at zero degrees relative to the beam direction, located at a distance 112.5 m from the nominal interaction point. The ZDC in the Pb-going direction is labeled ZNA.

Jet reconstruction in this analysis uses charged-particle tracks. Tracks are measured by the Inner Tracking System (ITS), a six-layer silicon vertex tracker, and the Time Projection Chamber (TPC). The tracking system acceptance covers $|\eta| < 0.9$ over the full azimuth, with tracks reconstructed in the range $0.15 < p_{\rm T} < 100\,{\rm GeV}/c$. Primary vertices are reconstructed offline by extrapolation of these tracks to the beam axis. Primary tracks are defined as reconstructed tracks with Distance of Closest Approach to the primary vertex in the transverse plane $DCA_{xy} < 2.4$ cm.

The analysis uses high-quality primary tracks that include at least one track point in the Silicon Pixel Detector (SPD), which comprises the two innermost layers of ITS. The azimuthal distribution of such high-quality tracks is non-uniform, however, due to the non-uniform acceptance of the SPD in this run. Azimuthal uniformity in the tracking acceptance is achieved by supplementing the high-quality tracks with complementary tracks that do not have a hit in the SPD, which constitute 4.3% of all primary tracks. The momentum resolution of complementary tracks, without an additional constraint, is lower than that of high-quality tracks. Complementary tracks are therefore refit, including the reconstructed primary vertex as a track point. Tracking efficiency for primary tracks is about 81% for $p_{\rm T} > 3\,{\rm GeV}/c$. Primary-track momentum resolution is 0.7% at $p_{\rm T} = 1\,{\rm GeV}/c$, 1.6% at $p_{\rm T} = 10\,{\rm GeV}/c$, and 4% at $p_{\rm T} = 50\,{\rm GeV}/c$. Further details on the track selection and tracking performance in this analysis are given in [23,68].

The MB trigger efficiency for non-single diffractive (NSD) collisions is $97.8 \pm 3.1\%$ [68,86]. Since this is a correlation analysis, no correction is applied for the trigger inefficiency. Timing cuts on the V0 and ZDC signals, which are applied offline, remove background events with vertices outside of the nominal p–Pb interaction region that arise from beam-gas interactions and interactions with satellite beam bunches [85].

Event pileup, due to multiple interactions in the triggered bunch crossing, is suppressed by rejecting events with multiple primary vertex candidates. For this procedure, a new set of primary vertex candidates is constructed from tracklets constructed solely from SPD hits ("SPD vertices"). SPD vertices have at least five SPD tracklets within $DCA < 1$ mm and lie within the expected envelope of p–Pb interaction points, with a distance not more than 3σ in z or 2σ in the xy plane from the centroid of the distribution. The minimum distance in z between SPD vertices is 8 mm. Events with multiple SPD vertices are rejected from further analysis. The EA-bias of the pileup rejection procedure is negligible, due to the large separation of pileup vertices in z and the requirement that each SPD vertex have at least five contributors. In this dataset, the average number of interactions per bunch crossing was $\mu \approx 0.3$–0.5%, and this pileup rejection procedure removes less than 0.15% of all events.

In addition, accepted events must have the primary vertex (defined above) with $|z_{\rm vtx}| < 10$ cm relative to the nominal center of the ITS along the beam axis. After all event selection cuts, the number of events in the analysis is 96×10^6, corresponding to an integrated luminosity of $46\,\mu{\rm b}^{-1}$.

Simulations are used to correct the raw data for instrumental effects, and to compare the corrected measurements to expectations from an event generator. Simulated events were generated for pp collisions at $\sqrt{s} = 5.02$ TeV using PYTHIA 6.425 with the Perugia 11 tune [87]. These events, labeled "particle-level," include all primary charged particles as defined in [88]. Following the procedure in [65], instrumental effects are calculated by passing particle-level events through a detailed model of the ALICE detector based on GEANT3 [89]. These events are reconstructed with the same procedures that are used for real data; the output of this process is labeled "detector-level." Comparison to data also uses a particle-level simulation of pp collisions at $\sqrt{s} = 5.02$ TeV generated with PYTHIA 8.215 Tune 4C [90]. All simulations take account of the nucleon–nucleon center-of-mass rapidity shift of the p–Pb data.

3. Event selection

This analysis is based on the semi-inclusive distribution of jets recoiling from a high-$p_{\rm T}$ trigger hadron. Event selection requires the presence of a high-$p_{\rm T}$ charged track, called the Trigger Track (TT), in a specified $p_{\rm T,trig}$ interval. Two exclusive event sets are defined, based on different TT intervals: $12 < p_{\rm T,trig} < 50\,{\rm GeV}/c$, denoted TT{12,50}, and $6 < p_{\rm T,trig} < 7\,{\rm GeV}/c$, denoted TT{6,7}.

The choice of the upper TT interval limits is driven by two competing factors: the hardening of the recoil jet $p_{\rm T}$-spectrum with increasing $p_{\rm T,trig}$, and the decrease of the inclusive hadron production cross section for increasing $p_{\rm T,trig}$. The choice of TT{12,50} provides the optimum kinematic reach and statistical precision of the normalized recoil jet spectrum for this dataset. The criteria for the lower TT interval, TT{6,7}, are that it be significantly lower in $p_{\rm T,trig}$, with correspondingly softer recoil jet spectrum, while still in the region in which inclusive hadron production can be well-described perturbatively using collinear fragmentation functions [91,92].

The fraction of such events in the MB population is 6.9×10^{-4} for TT{12,50} and 6.4×10^{-3} for TT{6,7}. However, an event may satisfy both the TT{6,7} and TT{12,50} selection criteria, since fragmentation of an energetic jet can generate hadrons in both TT selection intervals. A procedure is required to ensure exclusive, statistically independent datasets for the two TT-selected populations. In addition, optimization of the statistical precision of the analysis requires similar number of events in the two TT classes. The MB population was therefore divided randomly into two subsets, whose sizes are inversely proportional to the relative rate of the

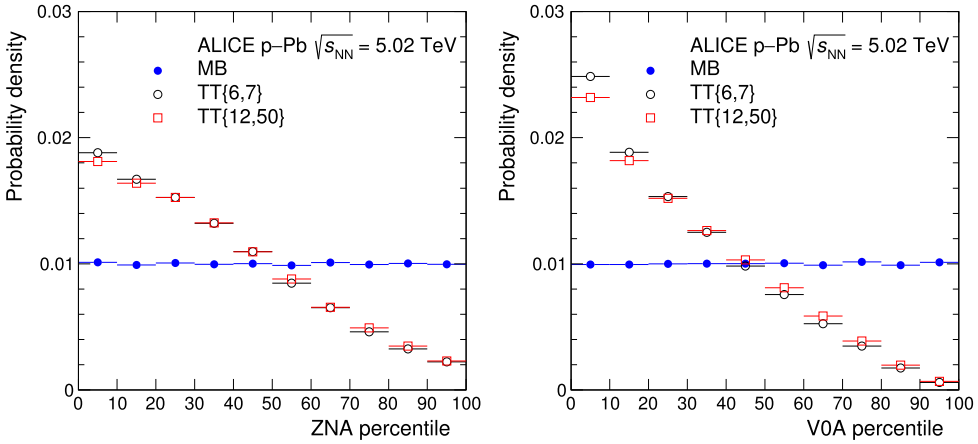

Fig. 1. Distribution of event activity EA in decile bins measured in ZNA (left) and V0A (right), for the MB event population and for event populations selected with the requirement of a high-p_T trigger hadron in the intervals $6 < p_{T,trig} < 7\,GeV/c$ (TT{6,7}) and $12 < p_{T,trig} < 50\,GeV/c$ (TT{12,50}). Large EA is to the left, with the 0–10% bin representing the largest EA, or highest amplitude signal in ZNA or V0A.

two TT selections: 90% of MB events are assigned to the TT{12,50} analysis, with the remaining 10% assigned to the TT{6,7} analysis.

An event can also contain multiple hadrons within a single TT interval, likewise arising from jet fragmentation. For events with at least one hadron satisfying TT{6,7}, the relative rate of two or more hadrons in an event satisfying TT{6,7} is 2.3%; the corresponding relative rate of multiple hadrons satisfying TT{12,50} is 5.3%. If an event contains more than one track in the assigned TT interval, the trigger hadron is chosen as the candidate with the highest p_T. The resulting p_T-distribution of trigger tracks is consistent with the shape of the inclusive hadron distribution within 2%. After the TT event selection procedure there are 63k events accepted that satisfy TT{6,7} and 60k events accepted that satisfy TT{12,50}.

A different procedure was employed in [9] for the case of multiple trigger candidates in a TT interval, where the trigger track was chosen randomly amongst the candidates. However, the analysis reported here has a wider range in p_T for the upper TT class, and random selection results in reduced level of agreement ($\sim$10%) of the trigger track p_T-distribution with the inclusive hadron spectrum shape. The full analysis was also carried out for this choice of procedure for trigger selection, and all resulting physics distributions agree with those of the primary analysis within the uncertainties.

Measurement of EA uses signals from V0A and ZNA. Classification of events in percentile intervals of the V0A and ZNA signal distributions is discussed in [56].

The ZNA threshold is set so that the detector is fully efficient for single neutrons. About 5% of accepted events do not have a ZNA signal above the detector threshold. These events correspond to p–Pb collisions in which the Pb-nucleus remnant is not accompanied by any beam-rapidity single neutrons. The distribution of mid-rapidity track multiplicity for these events resembles closely that for events with low but observable ZNA signal, and these events are therefore assigned to the bin with lowest ZNA signal.

Fig. 1 shows the distribution of EA measured by ZNA and V0A, in decile bins of signal amplitude. The decile bin limits are determined from their distributions in the MB population, with MB events therefore distributed uniformly in this projection by construction. The figure also shows V0A and ZNA distributions for event populations selected by the TT{6,7} and the TT{12,50} criteria. Requiring the presence of a high-p_T hadron trigger in an event is seen to induce a bias towards larger EA, corresponding to larger amplitude in both ZNA and V0A. A small dependence on the TT class (i.e. on $p_{T,trig}$) is also observed, with magnitude less than 10% of the overall bias, and with the TT-dependence slightly larger for V0A than for ZNA. Fig. 1 shows significant correlation between EA and the presence of a hard process in the central region.

For further analysis, events were assigned to wider percentile bins in ZNA or V0A, based on their MB distributions: 20% of the MB population with largest signal ("0–20%"), the next 30% ("20–50%"), and the remaining 50% with the lowest signal ("50–100%"). The bias imposed by TT selection, shown in Fig. 1, corresponds to different fractions of the TT-biased population: the nominal 0–20% ZNA interval corresponds to 0–35% of the TT-biased population; the nominal 20–50% ZNA interval corresponds to 35–74% of TT-biased; and the nominal 50–100% ZNA interval corresponds to 74–100% of TT-biased. Similar modification of percentile fractions due to TT bias is observed for the V0A signal.

The same events are used for the ZNA and V0A selections, so that the analyses using the two different EA metrics are not statistically independent.

4. Jet reconstruction

Several types of jet are used in the analysis, which we distinguish by the notation for jet p_T: $p_{T,jet}^{raw,ch}$ refers to the output of the jet reconstruction algorithm; $p_{T,jet}^{reco,ch}$ is $p_{T,jet}^{raw,ch}$ after subtraction of an estimated contribution to jet p_T of uncorrelated background; and $p_{T,jet}^{ch}$ refers to the fully corrected jet spectrum. For simulations, $p_{T,jet}^{part}$ refers to reconstructed charged-particle jets at the particle-level, and $p_{T,jet}^{det}$ refers to reconstructed charged-particle jets at the detector-level.

Jet reconstruction is carried out using the k_T and anti-k_T algorithms [83] with the boost-invariant p_T recombination scheme [93], using all accepted charged tracks with $p_T > 0.15\,GeV/c$. Jet area A_{jet} is calculated using the Fastjet algorithm [94] with ghost area 0.005.

Two jet reconstruction passes are carried out for each event. The first pass estimates the level of uncorrelated background energy in the event, while the second pass generates the set of jet candidates used in the physics analysis, with adjustment of their p_T using the estimated background level from the first pass.

In the first pass, the $p_{T,jet}^{raw,ch}$ distribution reconstructed by the k_T algorithm with $R = 0.4$ is used to estimate ρ, the magnitude of background energy per unit area [95],

Table 1
Contributions to the relative systematic uncertainty of the Δ_{recoil} distribution for $R = 0.2$ and 0.4 in EA-biased events based on ZNA.

	Δ_{recoil} syst. uncert. (%) ZNA 0–20%				Δ_{recoil} syst. uncert. (%) ZNA 50–100%			
$p_{\mathrm{T,jet}}^{\mathrm{ch}}$	15–20 GeV/c		40–50 GeV/c		15–20 GeV/c		40–50 GeV/c	
R	0.2	0.4	0.2	0.4	0.2	0.4	0.2	0.4
Unfolding algorithm	< 1	1.7	1.8	4.8	1.4	1.4	1.1	< 1
Unfolding prior	0.5	0.2	1.7	0.5	0.2	1.2	1.5	1.2
Binning of raw spectrum	1.1	2.4	0.5	1.2	1.0	1.2	2.1	2.2
ρ estimator	0.2	2.7	0.9	0.2	0.8	2.8	2.0	4.4
c_{Ref}	2.3	3.6	1.7	0.5	1.4	0.9	1.7	1.3
Track reconstruction efficiency	4.7	3.3	9.0	11	4.8	4.2	10	11
Track p_{T} resolution	0.6	0.6	1.0	1.7	0.6	0.6	1.0	1.7
Weak decays	< 1	< 1	< 1	< 1	< 1	< 1	< 1	< 1
Cumulative	5.4	6.3	9.6	12	5.4	5.6	11	12

$$\rho = \mathrm{median}_{k_{\mathrm{T}}\ \mathrm{jets}} \left\{ \frac{p_{\mathrm{T,jet}}^{\mathrm{raw,ch}}}{A_{\mathrm{jet}}} \right\}, \tag{1}$$

where the median is calculated by excluding the jet which has the trigger hadron as a constituent. A different ρ estimator [96] is utilized to assess the systematic uncertainties of this procedure.

The second jet reconstruction pass is carried out using the anti-k_{T} algorithm with $R = 0.2$ and 0.4. The value of $p_{\mathrm{T,jet}}^{\mathrm{raw,ch}}$ for each jet candidate from this step is then adjusted for the estimated background energy density [95],

$$p_{\mathrm{T,jet}}^{\mathrm{reco,ch}} = p_{\mathrm{T,jet}}^{\mathrm{raw,ch}} - A_{\mathrm{jet}} \cdot \rho. \tag{2}$$

A jet candidate from the second pass is accepted for further analysis if its area satisfies $A_{\mathrm{jet}} > 0.6\pi R^2$ [9,23], and its jet axis lies within $|\eta_{\mathrm{jet}}| < 0.9 - R$ and an azimuthal interval situated back-to-back with respect to the TT, $\Delta\varphi > \pi - 0.6$, where $\Delta\varphi = \varphi_{\mathrm{TT}} - \varphi_{\mathrm{jet}}$ and $0 < \Delta\varphi < \pi$. An event may have multiple accepted jet candidates.

For further analysis we follow the procedure used in [9], in which no rejection of individual jet candidates is carried out. Recoil jet distributions are accumulated for the selected event populations, and corrections for uncorrelated jet yield and for smearing and residual shift of $p_{\mathrm{T,jet}}^{\mathrm{ch}}$ due to uncorrelated background are carried out at the level of the ensemble-averaged distributions, as discussed below.

Jet energy resolution due to instrumental effects (JER) and jet energy scale (JES) uncertainty are similar to those in [9]. The JER is determined by comparing simulated jets at the particle and detector levels. The distribution of $(p_{\mathrm{T,jet}}^{\mathrm{det}} - p_{\mathrm{T,jet}}^{\mathrm{part}})/p_{\mathrm{T,jet}}^{\mathrm{part}}$ is asymmetric, with a sharp peak centered at zero and a tail to negative values [20]. Fit of a Gaussian function to the sharp peak gives $\sigma \simeq$ 2–3%, while the full distribution has RMS $\simeq$ 25%, with both quantities having no significant dependence on $p_{\mathrm{T,jet}}^{\mathrm{part}}$ and R. The JES uncertainty, which is due predominantly to uncertainty in tracking efficiency, is 4%, likewise with no significant dependence on $p_{\mathrm{T,jet}}^{\mathrm{ch}}$ and R. However, these values of JER and JES uncertainty, while helpful to characterize the jet measurement, are not used in the analysis. Corrections are carried out utilizing the full response matrix, which incorporates detailed distributions of all contributions to JER and JES uncertainty. The systematic uncertainties (Table 1) likewise take such factors fully into account.

5. Observable and raw data

The semi-inclusive h+jet distribution corresponds to the p_{T}-differential distribution of recoil jets normalized by the number of trigger hadrons, N_{trig},

$$\frac{1}{N_{\mathrm{trig}}} \frac{\mathrm{d}^2 N_{\mathrm{jets}}}{\mathrm{d}p_{\mathrm{T,jet}}^{\mathrm{ch}}\,\mathrm{d}\eta_{\mathrm{jet}}}\bigg|_{\substack{p_{\mathrm{T,trig}}\in\mathrm{TT} \\ \Delta\varphi\in\mathrm{recoil}}} = \frac{1}{\sigma^{\mathrm{pPb}\to\mathrm{h+X}}} \frac{\mathrm{d}^2\sigma^{\mathrm{pPb}\to\mathrm{h+jet+X}}}{\mathrm{d}p_{\mathrm{T,jet}}^{\mathrm{ch}}\,\mathrm{d}\eta_{\mathrm{jet}}}\bigg|_{\substack{\mathrm{h}\in\mathrm{TT} \\ \Delta\varphi\in\mathrm{recoil}}} \tag{3}$$

All accepted jets contribute to the distribution on the LHS. This distribution is equivalent to measurement of the ratio of two cross sections, as shown on the RHS: the coincidence cross section for both trigger hadron and recoil jet to be in the acceptance, divided by the inclusive production cross section for trigger hadrons. This expression applies to both the MB event population, and to event subsets selected by EA. The features of this observable and its theoretical calculations are discussed in detail in Refs. [9,20]. Here we consider two specific aspects of this distribution.

The first aspect is the bias imposed by the high-p_{T} hadron trigger. For collision systems in which jet quenching occurs, selection of high-p_{T} hadrons is thought to bias towards the fragments of jet that have experienced little quenching, due to the combined effect of jet energy loss and the shapes of the inclusive jet production and the jet fragmentation distributions [97–104]. If that is the case, then the hadron trigger bias in this measurement would be independent of EA. This conjecture is supported by ALICE measurements of inclusive hadron production in p–Pb collisions that find no significant yield modification in the trigger p_{T}-range of this measurement, for both the MB and EA-selected event populations [56,62]. The picture provided by current ATLAS and CMS hadron production measurements [60,63] is more complex, however. Further study of this conjecture requires additional measurements of inclusive hadron production in pp and p–Pb collisions, together with theoretical calculations incorporating jet quenching that accurately reproduce these measurements.

The second aspect is the effect of trigger hadron efficiency on the equality in Eq. (3). As noted in Sect. 3, the analysis requires selection of a single trigger hadron in each event. However, in a few percent of events there are multiple hadrons satisfying the TT selection criteria, of which only one is chosen as trigger. Consequently, not all hadrons that would contribute to measurement of the inclusive hadron cross section (first term on the RHS of Eq. (3)) also contribute to N_{trig} (first term on the LHS of Eq. (3)). However, as noted above, the shape of the trigger hadron p_{T}-distribution is consistent with that of the inclusive hadron spectrum within 2%. In other words, the trigger distribution used in practice samples the inclusive hadron distribution with efficiency less than unity but without p_{T}-dependent bias, within a precision of 2%. This same inefficiency also applies to the h+jet coincidence process in the second term on the LHS of Eq. (3), and it therefore cancels iden-

tically in the ratio. Equation (3) therefore remains valid for trigger selection efficiency less than unity.

The study of jet quenching using inclusive yields requires comparison of the inclusive distribution measured in heavy ion collisions to a reference distribution measured in a system in which quenching effects are not expected, usually pp collisions at the same $\sqrt{s_{\mathrm{NN}}}$. Such comparisons must account for the effect of multiple nucleon–nucleon collisions in each collision of heavy nuclei, which arises due to nuclear geometry. For inclusive distributions in p–Pb collisions this is accomplished by scaling inclusive cross sections for pp collisions by $\langle T_{\mathrm{pPb}} \rangle$, which is calculated by modeling based on Glauber theory under the assumption that EA is correlated with the collision geometry [56–60,62,63,65,66,68,69].

For the semi-inclusive distribution in Eq. (3), the reference distribution without nuclear effects is

$$\begin{aligned}
&\frac{1}{\sigma_{\mathrm{ref}}^{\mathrm{pPb}\to\mathrm{h+X}}} \frac{\mathrm{d}^2\sigma_{\mathrm{ref}}^{\mathrm{pPb}\to\mathrm{h+jet+X}}}{\mathrm{d}p_{\mathrm{T,jet}}^{\mathrm{ch}}\,\mathrm{d}\eta_{\mathrm{jet}}}\bigg|_{\substack{h\in\mathrm{TT}\\ \Delta\varphi\in\mathrm{recoil}}} \\
&= \frac{1}{\langle T_{\mathrm{pPb}} \rangle \cdot \sigma^{\mathrm{pp}\to\mathrm{h+X}}} \frac{\langle T_{\mathrm{pPb}} \rangle \cdot \mathrm{d}^2\sigma^{\mathrm{pp}\to\mathrm{h+jet+X}}}{\mathrm{d}p_{\mathrm{T,jet}}^{\mathrm{ch}}\,\mathrm{d}\eta_{\mathrm{jet}}}\bigg|_{\substack{h\in\mathrm{TT}\\ \Delta\varphi\in\mathrm{recoil}}} \\
&= \frac{1}{\sigma^{\mathrm{pp}\to\mathrm{h+X}}} \frac{\mathrm{d}^2\sigma^{\mathrm{pp}\to\mathrm{h+jet+X}}}{\mathrm{d}p_{\mathrm{T,jet}}^{\mathrm{ch}}\,\mathrm{d}\eta_{\mathrm{jet}}}\bigg|_{\substack{h\in\mathrm{TT}\\ \Delta\varphi\in\mathrm{recoil}}} . \qquad (4)
\end{aligned}$$

Since the scaling factors $\langle T_{\mathrm{pPb}} \rangle$ in the numerator and denominator cancel identically, the reference distribution for this observable has no dependence on $\langle T_{\mathrm{pPb}} \rangle$. In other words, this distribution is self-normalized, and measurement of jet quenching using this observable does not require Glauber modeling for the reference spectrum. In particular, the assumption that event activity is correlated with the collision geometry is not required.

A similar approach, utilizing a coincidence observable to measure jet quenching in high-multiplicity pp collisions, was recently proposed in [105].

Fig. 2, left panels, show recoil-jet distributions for $R = 0.4$ in p–Pb collisions with the 50–100% ZNA selection, and for $R = 0.2$ and 0.4 with the 0–20% ZNA selection. Distributions in EA intervals selected with V0A and with 20–50% ZNA are similar [106]. The distributions have non-zero yield for $p_{\mathrm{T,jet}}^{\mathrm{reco,ch}} < 0$, because regions of an event can have energy density less than ρ [9]. These distributions are significantly narrower in the region $p_{\mathrm{T,jet}}^{\mathrm{reco,ch}} < 0$ than those observed in central Pb–Pb collisions, where the uncorrelated component of the event is significantly larger [9].

Fig. 2, right panels, show ratios of the distributions for the two TT classes. The right panels also show the corresponding ratio for pp collisions at $\sqrt{s} = 5.02$ TeV, using simulated detector-level events generated with PYTHIA Perugia 11. For $p_{\mathrm{T,jet}}^{\mathrm{reco,ch}} \sim 0$ the two distributions agree within $\sim 10\%$ for both values of R, consistent with the expectation that yield in this region arises predominantly from processes that are uncorrelated with the trigger hadron [9]. At larger $p_{\mathrm{T,jet}}^{\mathrm{reco,ch}}$, the distribution for TT{12,50} exceeds that for TT{6,7}. This dependence of the recoil distribution on $p_{\mathrm{T,trig}}$ is expected from QCD-based considerations, since higher $p_{\mathrm{T,trig}}$ biases towards hard processes with higher Q^2 on average. Indeed, hardening of the semi-inclusive recoil jet distribution with increasing $p_{\mathrm{T,trig}}$ is also seen in the PYTHIA-generated ratios for pp collisions at $\sqrt{s} = 5.02$ TeV shown in the figure, and has been measured in pp collisions at $\sqrt{s} = 7$ TeV and observed in theoretical calculations based on NLO pQCD and on PYTHIA [9].

The PYTHIA-generated ratio for pp collisions reproduces well the ratio measured for low-EA p–Pb collisions (ZNA 50–100%, Fig. 2 upper right panel), while the level of agreement between the simulation and measurements is not as good for high-EA p–Pb collisions (ZNA 0–20%, Fig. 2, middle and bottom right panels). This occurs because there is larger uncorrelated background in high-EA than in low-EA p–Pb collisions.

The distribution of jet candidates that are uncorrelated with the trigger is independent of $p_{\mathrm{T,trig}}$, by definition. The distribution of correlated recoil jets can therefore be measured using the Δ_{recoil} observable, which is the difference of the two normalized recoil distributions [9],

$$\begin{aligned}
\Delta_{\mathrm{recoil}}\left(p_{\mathrm{T,jet}}^{\mathrm{ch}}\right) = &\frac{1}{N_{\mathrm{trig}}} \frac{\mathrm{d}^2 N_{\mathrm{jets}}}{\mathrm{d}p_{\mathrm{T,jet}}^{\mathrm{ch}}}\bigg|_{p_{\mathrm{T,trig}}\in\mathrm{TT_{Sig}}} \\
&- c_{\mathrm{Ref}} \cdot \frac{1}{N_{\mathrm{trig}}} \frac{\mathrm{d}^2 N_{\mathrm{jets}}}{\mathrm{d}p_{\mathrm{T,jet}}^{\mathrm{ch}}}\bigg|_{p_{\mathrm{T,trig}}\in\mathrm{TT_{Ref}}} , \qquad (5)
\end{aligned}$$

where $\mathrm{TT_{Sig}}$ and $\mathrm{TT_{Ref}}$ refer to Signal and Reference TT intervals, in this analysis corresponding to TT{12,50} and TT{6,7} respectively. Δ_{recoil} is normalized per unit η_{jet}, notation not shown.

The Reference spectrum in Δ_{recoil} is scaled by the factor c_{Ref} to account for the invariance of the jet density with TT-class, as indicated by comparison of the spectrum integrals in Fig. 2 and the larger yield of Signal spectrum at high $p_{\mathrm{T,jet}}^{\mathrm{reco,ch}}$ [9]. The value of c_{Ref} in this analysis is taken as the ratio of the Signal and Reference spectra in the bin $0 < p_{\mathrm{T,jet}}^{\mathrm{reco,ch}} < 1$ GeV/c, as shown by the arrow in Fig. 2, right panels. The value of c_{Ref} lies between 0.92 and 0.99 for the various spectra. Additional variation in the value of c_{Ref} was used to assess systematic uncertainties.

We note that the $\mathrm{TT_{Ref}}$ distribution includes correlated recoil jet yield, so that the subtraction in Eq. (5) removes both the trigger-uncorrelated yield and the $\mathrm{TT_{Ref}}$-correlated yield. The Δ_{recoil} observable is therefore a differential, not absolute, measurement of the recoil spectrum [9], though the $\mathrm{TT_{Ref}}$ component is significantly smaller than that in the $\mathrm{TT_{Sig}}$ component over most of the $p_{\mathrm{T,jet}}^{\mathrm{reco,ch}}$ range. The Δ_{recoil} distributions in Fig. 2 lie significantly below the TT-specific distributions for $p_{\mathrm{T,jet}}^{\mathrm{reco,ch}} < 5$ GeV/c but agree with the TT{12,50} distribution within 15% for $p_{\mathrm{T,jet}}^{\mathrm{reco,ch}} > 15$ GeV/c. These features indicate that the region of negative and small positive $p_{\mathrm{T,jet}}^{\mathrm{reco,ch}}$ is dominated by uncorrelated jet yield, while the region for large positive $p_{\mathrm{T,jet}}^{\mathrm{reco,ch}}$ is dominated by recoil jet yield that is correlated with $\mathrm{TT_{Sig}}$.

One contribution to uncorrelated background is jet yield due to Multiple Partonic Interactions (MPI), which can occur when two independent high-Q^2 interactions in the same p–Pb collision generate the trigger hadron and a jet in the recoil acceptance. Since the two interactions are independent, the recoil jet distribution generated by MPI will be independent of $p_{\mathrm{T,trig}}$, by definition, and will be removed from Δ_{recoil} by the subtraction. No correction of Δ_{recoil} for the contribution of MPI is therefore needed in the analysis.

The raw Δ_{recoil} distributions, such as those in Fig. 2, must still be corrected for jet momentum smearing due to instrumental effects and local background fluctuations, and for jet reconstruction efficiency. Jet quenching effects are measured by comparing the corrected Δ_{recoil} distributions for different EA classes, and at different R.

6. Corrections

Corrections for instrumental effects and local background fluctuations are carried out using unfolding methods [107–109]. The measured distribution $\Delta_{\mathrm{recoil}}^{\mathrm{M}}$ is related to the true distribution $\Delta_{\mathrm{recoil}}^{\mathrm{T}}$ by a linear transformation,

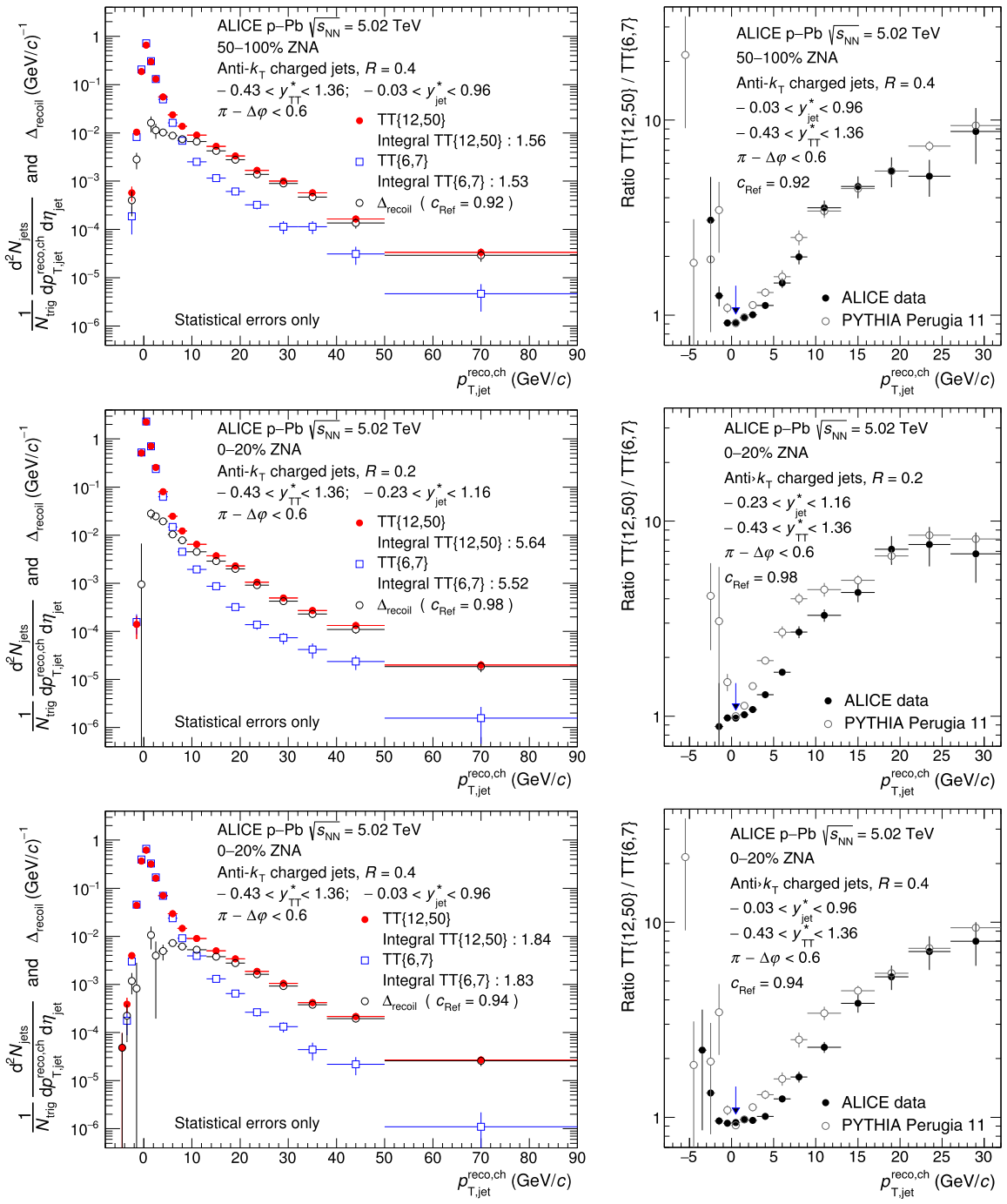

Fig. 2. Uncorrected semi-inclusive distributions of charged jets recoiling from a high-p_T hadron trigger in p–Pb collisions at $\sqrt{s_{NN}} = 5.02$ TeV with the EA selection of 50–100% in ZNA for $R = 0.4$ (top panels), and with the EA selection of 0–20% in ZNA for $R = 0.2$ (middle panels) and $R = 0.4$ (bottom panels). The acceptance for TT and recoil jets in the CM frame are denoted y^*_{TT} and y^*_{jet}, respectively. Left panels: raw distributions for TT{12,50} (red circles) and TT{6,7} (blue boxes), and the corresponding Δ_{recoil} distribution (Eq. (5), black circles). Right panels: ratio of yields for TT{12,50}/TT{6,7} measured by ALICE in p–Pb collisions and calculated using detector level PYTHIA Perugia 11 simulation of pp collisions at $\sqrt{s} = 5.02$ TeV. The PYTHIA-generated ratios in the top right and bottom right panels are the same. The arrow indicates the 0–1 GeV/c bin which is used to calculate c_{Ref}. The uncertainties are statistical only. (For interpretation of the colors in the figure(s), the reader is referred to the web version of this article.)

$$\Delta^{M}_{recoil}(p^{reco,ch}_{T,jet}) = R_{full}(p^{reco,ch}_{T,jet}, p^{part}_{T,jet}) \otimes \left[\text{eff}(p^{part}_{T,jet}) \cdot \Delta^{T}_{recoil}(p^{part}_{T,jet}) \right], \quad (6)$$

where $\text{eff}(p^{part}_{T,jet})$ is the jet reconstruction efficiency and R_{full} is the cumulative response matrix excluding jet reconstruction efficiency. The explicit specification of jet reconstruction efficiency in this expression, distinct from the unfolding step, makes interpretation of the unfolding procedure more transparent. $R_{full}(p^{reco,ch}_{T,jet}, p^{part}_{T,jet})$ is further assumed to factorize as the product of separate response matrices for background fluctuations and instrumental response,

$$R_{full}(p^{reco,ch}_{T,jet}, p^{part}_{T,jet}) = R_{bkgd}(p^{reco,ch}_{T,jet}, p^{det}_{T,jet}) \otimes R_{instr}(p^{det}_{T,jet}, p^{part}_{T,jet}). \quad (7)$$

The matrix R_{full} can be close to singular, in which case the solution of Eq. (6) via direct inversion of R_{full} generates large fluctuations in central values and large variance due to the statistical variation in

$\Delta^{\mathrm{M}}_{\mathrm{recoil}}(p^{\mathrm{reco,ch}}_{\mathrm{T,jet}})$ and R_{full} [107]. An approximate solution of Eq. (6) that is physically more meaningful is obtained by regularized unfolding, which imposes a smoothness constraint on the solution. Unfolding in this analysis is carried out using approaches based on Singular Value Decomposition (SVD) [108] and on Bayes' Theorem [109], as implemented in the RooUnfold package [110].

The instrumental response matrix, R_{instr}, is calculated from the simulated detector response applied to events generated by PYTHIA for pp collisions at $\sqrt{s} = 5.02$ TeV. Jets at the particle-level and detector-level are matched in (η, ϕ) space by selecting the detector-level jet that is closest to the particle-level jet, and vice versa. An entry in R_{instr} is made for every matched pair. The R_{instr} matrix is normalized such that, for each bin in $p^{\mathrm{part}}_{\mathrm{T,jet}}$, the sum over all bins in $p^{\mathrm{det}}_{\mathrm{T,jet}}$ is unity. In practice, however, the matching probability is less than unity, which is accounted for in Eq. (6) by the efficiency factor $\mathrm{eff}(p^{\mathrm{part}}_{\mathrm{T,jet}})$. No dependence of R_{instr} on EA of the p–Pb event population was observed.

The background response matrix, R_{bkgd}, is calculated by embedding single tracks with transverse momentum $p^{\mathrm{embed}}_{\mathrm{T}}$ into real p–Pb events that contain a TT [9]. The relative azimuthal angle between the embedded track and the TT is in the range $[\pi/4, 3\pi/4]$, to minimize overlap of the embedded track with the jet containing TT and with true recoil jets. These hybrid events are analyzed with the same procedures used for real data, and the jet containing the embedded track is identified. Smearing of jet candidate p_{T} due to background fluctuations is quantified by the distribution of

$$\delta p_{\mathrm{T}} = p^{\mathrm{reco,ch}}_{\mathrm{T,jet}} - p^{\mathrm{embed}}_{\mathrm{T}}, \tag{8}$$

where $p^{\mathrm{reco,ch}}_{\mathrm{T,jet}}$ refers to the jet containing the embedded track. R_{bkgd}, the probability distribution of δp_{T}, is calculated separately for the MB population and for the various event populations selected by EA. Embedding of PYTHIA-generated jets rather than single tracks yields very similar δp_{T} distributions.

Unfolding follows the procedure described in [23]. The input to unfolding is the measured distribution $\Delta^{\mathrm{M}}_{\mathrm{recoil}}(p^{\mathrm{reco,ch}}_{\mathrm{T,jet}})$ in the range $1 < p^{\mathrm{reco,ch}}_{\mathrm{T,jet}} < 90$ GeV/c. The unfolding procedure requires specification of a prior distribution. For the primary analysis, the prior is the Δ_{recoil} distribution calculated with PYTHIA8 tune 4C [90] for pp collisions at $\sqrt{s} = 5.02$ TeV. Regularization of SVD unfolding utilizes a statistical test to determine the transition between random fluctuations and statistically significant components of the d-vector [108], which is achieved typically with regularization parameter $k = 4$. For regularization of Bayesian unfolding, convergence is determined by the stability of the unfolded solution for successive iterations, which is achieved typically by the second iteration.

For both unfolding approaches, consistency of the solution is checked by backfolding, i.e. smearing the unfolded distribution with R_{full} and comparing the result with the $\Delta^{\mathrm{M}}_{\mathrm{recoil}}$ distribution. Since regularization suppresses oscillating components of the solution, the backfolded and $\Delta^{\mathrm{M}}_{\mathrm{recoil}}$ distributions will in general not be identical. Consistency of unfolding is imposed by requiring that the difference between the backfolded and $\Delta^{\mathrm{M}}_{\mathrm{recoil}}$ distributions in each bin be less than 3σ, based on $\Delta^{\mathrm{M}}_{\mathrm{recoil}}$ statistical errors; otherwise, the solution is rejected.

Closure of the unfolding procedure was verified by a test in which the response matrix, the Δ_{recoil} distribution, and the prior were generated by statistically independent sets of PYTHIA-generated events for pp collisions at $\sqrt{s} = 5.02$ TeV. The response matrix and the spectrum were generated using PYTHIA6 Perugia-11, while the prior was generated using PYTHIA8 tune 4C. The Δ_{recoil} distribution from this test agrees with the input particle-level distribution to better than 5%.

Correction for jet reconstruction efficiency is applied after the unfolding step by scaling the unfolded Δ_{recoil} distribution by $1/\mathrm{eff}(p^{\mathrm{ch}}_{\mathrm{T,jet}})$. The value of $\mathrm{eff}(p^{\mathrm{ch}}_{\mathrm{T,jet}})$ is 0.96 at $p^{\mathrm{ch}}_{\mathrm{T,jet}} = 15$ GeV/c and 0.98 at $p^{\mathrm{ch}}_{\mathrm{T,jet}} = 60$ GeV/c.

7. Systematic uncertainties

The systematic uncertainties of the Δ_{recoil} distribution are assessed by varying the components of the correction procedure. The most significant systematic uncertainties are due to the following:

- Regularization of unfolding: for SVD, vary k by ± 2 relative to its value in the primary analysis; for Bayesian unfolding, use the first three iterations;
- Unfolding prior: generate prior distributions with PYTHIA6 and PYTHIA8; for additional variation take the difference between the priors from the two PYTHIA versions and vary them by its magnitude but with opposite sign; use the unfolded solution based on the iterative Bayesian approach as prior for SVD-based unfolding;
- Binning of distributions: use three different choices of binning, with corresponding variation in spectrum limits;
- Calculation of ρ: utilize a modified procedure [65,81,96] that accounts for sparse regions of the event, instead of the area-based approach (Eq. (1));
- c_{Ref} variation: use as upper limit $c_{\mathrm{Ref}} = 1$, in which the reference recoil jet spectrum is not scaled. For the lower limit, double the value of $(1 - c_{\mathrm{Ref}})$ from the primary analysis, giving $c_{\mathrm{Ref}} = 0.95$ for $R = 0.2$ and $c_{\mathrm{Ref}} = 0.90$ for $R = 0.4$. The systematic uncertainty band corresponds to the largest deviation from all such variations of the unfolded spectrum, relative to the spectrum resulting from the c_{Ref} choice of the primary analysis;
- Tracking efficiency: vary $\pm 4\%$ relative to nominal value [65];
- Track momentum resolution: extract systematic uncertainty of momentum resolution from azimuthal variation of the inclusive charged-track distribution; vary R_{instr} accordingly.

The correction for secondary vertex tracks due to weak decays makes a smaller contribution to the systematic uncertainty than the above sources.

There is a difference in the response matrix for different selections of EA, due to the different magnitude of uncorrelated background induced by such a selection. The correction procedure accounts for this difference. However, there may be a residual correlation between the EA-bias and TT-bias in the calculation of the response. This correlation was explored by calculating the response matrix with the appropriate EA-selected data, both with and without TT-bias. The corrected spectra resulting from the two response matrices differ by less than 2% for all $p^{\mathrm{ch}}_{\mathrm{T,jet}}$, R, and EA-selection. This is however a check, not a systematic uncertainty, since the response matrix for the analysis is properly calculated using the TT-bias, and it does not contribute to the systematic uncertainty of the measurement.

The EA-bias induced by the TT{6,7} and TT{12,50} requirements are similar, and the δp_{T} distributions generated for events with the two TT requirements are likewise similar. This variation in the δp_{T} distribution generates variation of less that 1% in the corrected spectrum, after unfolding.

Statistical fluctuations of the raw data influence the quantitative assessment of the systematic uncertainties arising from these sources. We utilize the following procedure to minimize such effects. For each source of uncertainty, several randomized instances of the raw Δ_{recoil} spectrum are generated by variation about the

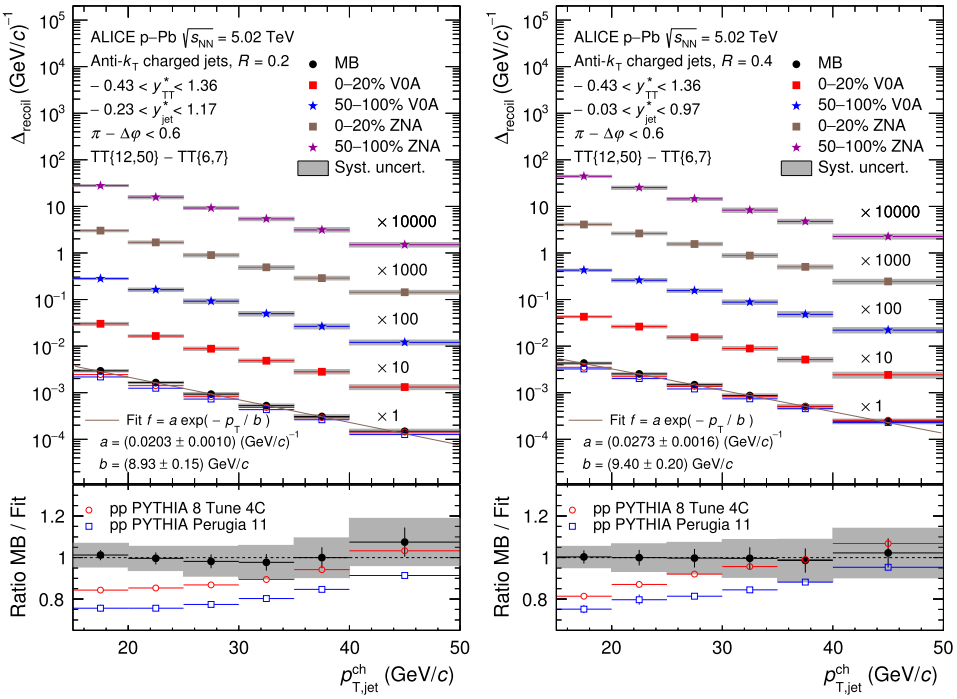

Fig. 3. Corrected Δ_{recoil} distributions measured for p–Pb collisions at $\sqrt{s_{NN}} = 5.02$ TeV, for the MB and EA-selected populations. The acceptance for TT and recoil jets in the CM frame are denoted y^*_{TT} and y^*_{jet}, respectively. Left panels: $R = 0.2$; right panels: $R = 0.4$. Also shown are Δ_{recoil} distributions for pp collisions at $\sqrt{s} = 5.02$ TeV simulated by PYTHIA 6 Tune Perugia 11 and PYTHIA 8 Tune 4C. The solid line in the upper panels is the fit of an exponential function to the p–Pb distribution, with fit parameters as specified. Lower panels: ratio of p–Pb MB and pp distributions to the fit function.

measured central value in each bin using a Gaussian distribution, with σ equal to the uncorrelated statistical error in the bin. Each randomized instance is analyzed using (i) corrections for the primary analysis (see Sect. 6), and (ii) corrections that include a systematic variation. For each randomized instance, the ratio of corrected Δ_{recoil} spectra resulting from (ii) and (i) is formed. The systematic uncertainty in each $p^{ch}_{T,jet}$-bin is defined as the median of the distribution of ratios obtained from all randomized instances.

Table 1 gives representative systematic uncertainties for $R = 0.2$ and $R = 0.4$ in EA-biased events based on ZNA. The cumulative systematic uncertainty is calculated by adding contributions from all systematic sources in quadrature. For $p^{ch}_{T,jet} = 15$–20 GeV/c, several components contribute with similar magnitude. For $p^{ch}_{T,jet} = 40$–50 GeV/c, the cumulative uncertainty is due predominantly to the uncertainty in tracking efficiency. Similar uncertainties are obtained for event selection using the EA bias based on V0A.

The systematic uncertainty of the ratio of Δ_{recoil} distributions was obtained similarly, taking into account the correlated uncertainties of numerator and denominator.

8. Results

Fig. 3, upper panels, show the corrected Δ_{recoil} distributions for p–Pb collisions at $\sqrt{s_{NN}} = 5.02$ TeV for the MB event population and for populations selected by EA using ZNA and V0A, and for pp collisions at $\sqrt{s} = 5.02$ TeV simulated by PYTHIA. The upper panels also show the result of a fit to the p–Pb MB distributions by an exponential function, $a \cdot \exp\left(-p^{ch}_{T,jet}/b\right)$.

The PYTHIA-generated distributions for pp collisions are presented only for comparison and are not utilized in the jet quenching analysis. Fig. 3, lower panels, show the ratio of the measured p–Pb MB and PYTHIA-generated pp distributions to the fit distribution. The central values of the PYTHIA-generated distributions for pp collisions lie below those of the p–Pb data, with a difference of 25% for $p^{ch}_{T,jet} < 20$ GeV/c. PYTHIA 8 tune 4C agrees better with the p–Pb data, notably at the highest $p^{ch}_{T,jet}$ and for $R = 0.4$. For pp collisions at $\sqrt{s} = 7$ TeV, PYTHIA-generated Δ_{recoil} distributions have central values that are in good agreement with data [9]. We note, however, that the $p_{T,trig}$ intervals in the two analyses are different: this analysis uses TT{12,50}, whereas that in ref. [9] used TT{20,50}. Reanalysis of the pp 7 TeV data with the trigger selection TT{12,50} shows a similar level of agreement with PYTHIA as that seen in Fig. 3 [106]. We also note that at present there are significant uncertainties in the light hadron fragmentation functions at LHC energies [91,92], which may affect hadron trigger selection in the PYTHIA calculation and thereby contribute to the differences between PYTHIA and data seen in the figure.

The Δ_{recoil} distributions for EA-selected event populations and for the MB population shown in Fig. 3 are all qualitatively similar. Measurement of the dependence of the Δ_{recoil} distribution on EA selection is therefore carried out using the ratios of such distributions, denoted R_{EA}, to maximize the sensitivity to variations with EA.

Fig. 4 shows ratios of the Δ_{recoil} distributions for EA-selected event populations, with $R = 0.2$ and 0.4. Since the numerator and denominator come from different, exclusive intervals in EA, they are statistically independent in each panel. However, some systematic uncertainties are correlated between numerator and denominator, which has been taken into account in the systematic uncertainty of the ratio. Note that the same dataset is used for $R = 0.2$ and $R = 0.4$, and for the ZNA and V0A selections, so that the results shown in the different panels are correlated.

Jet quenching may result in transport of jet energy out of the jet cone, resulting in suppression of the Δ_{recoil} distribution at fixed $p^{ch}_{T,jet}$. Under the assumptions (i) that jet quenching is more likely to occur in events with larger EA, and (ii) that the hadron trigger bias is independent of EA (Sect. 5), this effect corresponds to sup-

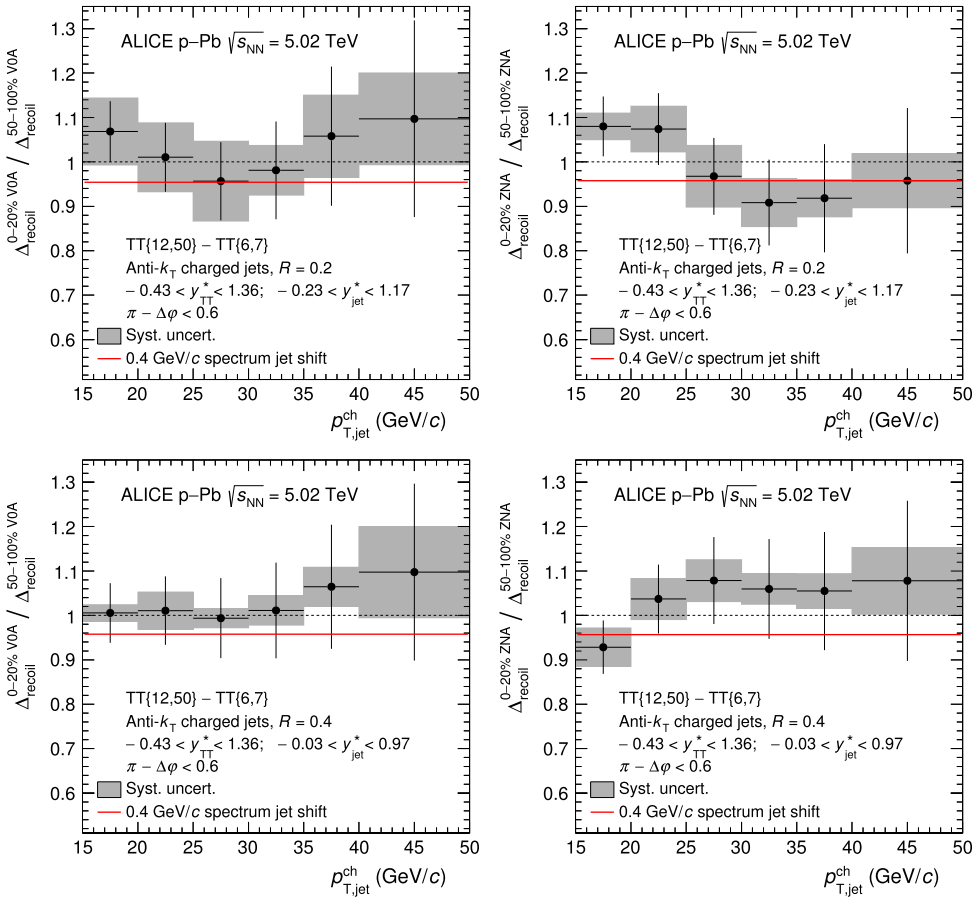

Fig. 4. Ratio of Δ_{recoil} distributions for events with high and low EA measured in p–Pb collisions at $\sqrt{s_{NN}} = 5.02$ TeV. Left panels: V0A 0–20% / 50–100%; right panels: ZNA 0–20% / 50–100%. Upper panels: $R = 0.2$; lower panels: $R = 0.4$. The grey boxes show the systematic uncertainty of the ratio, which takes into account the correlated uncertainty of numerator and denominator. The red line indicates the ratio for a p_T-shift of the high-EA distribution of -0.4 GeV/c.

pression below unity of the ratios in Fig. 4. However, in all panels the ratio is consistent with unity within the statistical error and the systematic uncertainty at all $p^{ch}_{T,jet}$, indicating that jet quenching effects are negligible relative to the uncertainties.

These data can nevertheless provide a limit on the magnitude of medium-induced energy transport to large angles. In order to extract a limit, we parameterize the 0–20% and 50–100% EA-selected Δ_{recoil} distributions with the exponential function used in Fig. 3, and assume that the slope parameter b is the same for the two distributions. We also assume that the average magnitude of energy transported out-of-cone is independent of $p^{ch}_{T,jet}$, which is consistent with the observation that the ratios R_{EA} in Fig. 4 are independent of $p^{ch}_{T,jet}$ within uncertainties. The assumption that the average magnitude of out-of-cone radiation is independent of $p^{ch}_{T,jet}$ is likewise consistent with Δ_{recoil} measurements in Pb–Pb collisions at 2.76 TeV [9]. Consideration of a more complex dependence on $p^{ch}_{T,jet}$ is beyond the scope of this phenomenological study.

The ratios R_{EA} are then expressed in terms of an average shift $\bar{s}$ in $p^{ch}_{T,jet}$ between low and high EA events, where $\bar{s} = -b \cdot \ln(R_{EA})$. Fits to Δ_{recoil} for $R = 0.4$ over the range $15 < p^{ch}_{T,jet} < 50$ GeV/c give $b = 9.26 \pm 0.33$ GeV/c for 50–100% ZNA and $b = 9.05 \pm 0.30$ GeV/c for 50–100% V0A. Fits to the ratios in Fig. 4 then give $\bar{s} = (-0.12 \pm 0.35_{stat} \pm 0.03_{syst})$ GeV/c for 0–20% ZNA, and $\bar{s} = (-0.06 \pm 0.34_{stat} \pm 0.02_{syst})$ GeV/c for 0–20% V0A, both of which are consistent with zero within uncertainties. Fits to narrower ranges in $p^{ch}_{T,jet}$ give similar results.

These values are to be compared with the shift $\bar{s} = (8 \pm 2_{stat})$ GeV/c measured in central Pb–Pb collisions at $\sqrt{s_{NN}} = 2.76$ TeV for $R = 0.5$ [9], indicating significant medium-induced energy transport to large angles in that collision system. This comparison of out-of-cone energy transport in p–Pb and Pb–Pb collisions supports theoretical calculations which predict much smaller jet quenching effects in p–Pb relative to Pb–Pb collisions [52,54], and disfavors the calculation which predicts strong jet quenching in small systems [53].

The measured value of $\bar{s}$ provides a constraint on the magnitude of out-of-cone energy transport due to jet quenching in p–Pb collisions. We calculate this constraint as the linear sum of the central value of $\bar{s}$, the one-sided 90% confidence upper limit of its statistical error, and the absolute value of its systematic uncertainty. For jets with $R = 0.4$ in the range $15 < p^{ch}_{T,jet} < 50$ GeV/c, the medium-induced charged energy transport out of the jet cone for events with high V0A or high ZNA is less than 0.4 GeV/c, at 90% confidence. The red line in each panel of Fig. 4 shows the ratio for a p_T-shift of -0.4 GeV/c of the high-EA distribution relative to the low-EA distribution.

9. Comparison to other measurements

The EA-selected Δ_{recoil} distribution ratios in Fig. 4 are consistent with unity in the range $15 < p^{ch}_{T,jet} < 50$ GeV/c. These distributions therefore have no significant dependence on EA, in agreement with inclusive jet measurements for p–Pb collisions at $\sqrt{s_{NN}} = 5.02$ TeV by ALICE [68], but in contrast to such measure-

Table 2
Comparison of R_{CP} and R^*_{CP} for inclusive jet production in asymmetric collisions at RHIC and the LHC. See text for details.

Collision system	Comparison of spectra	$p_{T,jet}$ (GeV/c)	R_{CP} or R^*_{CP}
d–Au, pp $\sqrt{s_{NN}} = 0.2$ TeV [59]	d–Au 0–20%/60–88%	16	$R_{CP} = 0.71 \pm 0.01_{stat} \pm 0.03_{sys}$
		32	$R_{CP} = 0.54 \pm 0.04_{stat} \pm 0.06_{sys}$
	pp w/wo -0.6 GeV/c shift	15	$R^*_{CP} = 0.79$
		30	$R^*_{CP} = 0.85$
p–Pb $\sqrt{s_{NN}} = 5.02$ TeV $y^* = 0.3$ [66]	p–Pb 0–10%/60–90%	57	$R_{CP} = 1.09 \pm 0.02_{stat} \pm 0.03_{sys}$
		113	$R_{CP} = 0.93 \pm 0.01_{stat} \pm 0.02_{sys}$
	p–Pb MB w/wo -0.6 GeV/c shift	50	$R^*_{CP} = 0.95$
		110	$R^*_{CP} = 0.97$

ments in d–Au collisions at $\sqrt{s_{NN}} = 200$ GeV by PHENIX [59] and in p–Pb collisions at $\sqrt{s_{NN}} = 5.02$ TeV by ATLAS [66], which exhibit strong dependence on EA. In this section we explore whether these inclusive and coincidence measurements can provide a consistent picture of jet quenching in asymmetric systems.

We first note that these measurements differ in several aspects, and that their detailed comparison requires calculations based on theoretical models of jet quenching that are beyond the scope of this paper. Here we explore a more limited question, whether the inclusive jet measurements are also consistent with a p_T-independent limit of out-of-cone charged-energy transport of 0.4 GeV/c. Since the ALICE inclusive jet measurement does not find an EA-dependence, it is consistent with such a limit by construction, without the need for additional calculation. We therefore focus in the rest of this section on comparison to the PHENIX and ATLAS inclusive jet measurements.

To do so, we compare the effect of a p_T-independent shift of the inclusive spectra to the measured EA-dependence of R_{CP}, which is the ratio of inclusive jet spectra for event populations identified as "central" and "peripheral", with the spectra scaled by $\langle T_{pPb} \rangle$ or $\langle T_{dAu} \rangle$. Since the inclusive spectra are measured with fully-reconstructed jets, including neutral energy, we increase the 90% confidence limit for out-of-cone energy transport to the value 0.6 GeV/c. Note in addition that the choice of percentile binning differs in the various measurements, which cannot be accounted for directly in the comparison; this difference should also be borne in mind when comparing the measurements.

The effect of the p_T-shift on jet yield depends upon the inclusive spectrum shape. In order to assess this effect we select a representative spectrum for each data set, impose a p_T-independent shift of -0.6 GeV/c on this spectrum, and calculate R^*_{CP}, the ratio of distributions with and without the shift. Since R^*_{CP} represents a 90% confidence limit, no uncertainty is assigned to it.

Table 2 compares R^*_{CP} to the values of EA-selected R_{CP} measured in asymmetric collisions at RHIC and the LHC. While some values are in agreement, R^*_{CP} and R_{CP} have opposite dependence on $p_{T,jet}$ for both datasets. Within the limits of this comparison, a $p^{ch}_{T,jet}$-independent out-of-cone charged-energy transport of 0.4 GeV/c is not consistent with measurements of R_{CP} for inclusive jet production in EA-selected d–Au collisions at RHIC and p–Pb collisions at the LHC.

Effects other than jet quenching in the final state can modify jet yields in nuclear collisions, in particular the initial-state effects of shadowing and energy loss in cold matter [55,111]. In addition, calculation of the Glauber scaling factor for inclusive measurements may be affected by fluctuations and dynamical correlations between a high Q^2 process and the soft observables used to tag EA [56,70–80]. Such non-quenching effects could be the origin of the inconsistency observed here in the EA-dependence of inclusive and coincidence jet measurements, since inclusive and coincidence observables have different sensitivity to initial-state effects, and Glauber scaling is required only for inclusive observables.

10. Summary

We have reported measurements of the semi-inclusive distribution of charged jets recoiling from a high-p_T hadron trigger in p–Pb collisions at $\sqrt{s_{NN}} = 5.02$ TeV, selected by event activity in forward (Pb-going) charged multiplicity and zero-degree neutral energy. Interpretation of this coincidence observable does not require the assumption that event activity is correlated with collision geometry, with the corresponding uncertainties of Glauber modeling. It provides a new probe of jet quenching in p–Pb collisions that is systematically different from quenching measurements based on inclusive jet production.

No significant difference is observed in recoil jet distributions for different event activity. This measurement provides a limit on out-of-cone energy transport due to jet quenching in p–Pb collisions at the LHC of less that 0.4 GeV/c at 90% confidence for jet radius $R = 0.4$. Comparison of this measurement to theoretical calculations favors models with little or no energy loss in small systems. Comparison to inclusive jet measurements in small systems at RHIC and LHC indicates that the inclusive jet yield modification observed in EA-selected populations is not consistent with jet quenching. Future p–Pb measurements at the LHC, with higher statistical precision and greater kinematic reach, will provide more stringent limits on jet quenching in light systems.

Acknowledgements

The ALICE Collaboration would like to thank all its engineers and technicians for their invaluable contributions to the construction of the experiment and the CERN accelerator teams for the outstanding performance of the LHC complex. The ALICE Collaboration gratefully acknowledges the resources and support provided by all Grid centers and the Worldwide LHC Computing Grid (WLCG) collaboration. The ALICE Collaboration acknowledges the following funding agencies for their support in building and running the ALICE detector: A. I. Alikhanyan National Science Laboratory (Yerevan Physics Institute) Foundation (ANSL), State Committee of Science and World Federation of Scientists (WFS), Armenia; Austrian Academy of Sciences and Nationalstiftung für Forschung, Technologie und Entwicklung, Austria; Ministry of Communications and High Technologies, National Nuclear Research Center, Azerbaijan; Conselho Nacional de Desenvolvimento Científico e Tecnológico (CNPq), Universidade Federal do Rio Grande do Sul (UFRGS), Financiadora de Estudos e Projetos (Finep) and Fundação de Amparo à Pesquisa do Estado de São Paulo (FAPESP), Brazil; Ministry of Science & Technology of China (MSTC), National Natural Science Foundation of China (NSFC) and Ministry of Education of China (MOEC), China; Ministry of Science, Edu-

cation and Sports and Croatian Science Foundation, Croatia; Ministry of Education, Youth and Sports of the Czech Republic, Czech Republic; The Danish Council for Independent Research Natural Sciences, the Carlsberg Foundation and Danish National Research Foundation (DNRF), Denmark; Helsinki Institute of Physics (HIP), Finland; Commissariat à l'Energie Atomique (CEA) and Institut National de Physique Nucléaire et de Physique des Particules (IN2P3) and Centre National de la Recherche Scientifique (CNRS), France; Bundesministerium für Bildung, Wissenschaft, Forschung und Technologie (BMBF) and GSI Helmholtzzentrum für Schwerionenforschung GmbH, Germany; General Secretariat for Research and Technology, Ministry of Education, Research and Religions, Greece; National Research, Development and Innovation Office, Hungary; Department of Atomic Energy, Government of India (DAE), Department of Science and Technology, Government of India (DST), University Grants Commission, Government of India (UGC) and Council of Scientific and Industrial Research (CSIR), India; Indonesian Institute of Science, Indonesia; Centro Fermi – Museo Storico della Fisica e Centro Studi Ricerche Enrico Fermi and Instituto Nazionale di Fisica Nucleare (INFN), Italy; Institute for Innovative Science and Technology, Nagasaki Institute of Applied Science (IIST), Japan Society for the Promotion of Science (JSPS) KAKENHI and Japanese Ministry of Education, Culture, Sports, Science and Technology (MEXT), Japan; Consejo Nacional de Ciencia y Tecnología (CONACYT), through Fondo de Cooperación Internacional en Ciencia y Tecnología (FONCICYT) and Dirección General de Asuntos del Personal Academico (DGAPA), Mexico; Nederlandse Organisatie voor Wetenschappelijk Onderzoek (NWO), Netherlands; The Research Council of Norway, Norway; Commission on Science and Technology for Sustainable Development in the South (COMSATS), Pakistan; Pontificia Universidad Católica del Perú, Peru; Ministry of Science and Higher Education and National Science Centre, Poland; Korea Institute of Science and Technology Information and National Research Foundation of Korea (NRF), Republic of Korea; Ministry of Education and Scientific Research, Institute of Atomic Physics and Romanian National Agency for Science, Technology and Innovation, Romania; Joint Institute for Nuclear Research (JINR), Ministry of Education and Science of the Russian Federation and National Research Centre Kurchatov Institute, Russia; Ministry of Education, Science, Research and Sport of the Slovak Republic, Slovakia; National Research Foundation of South Africa, South Africa; Centro de Aplicaciones Tecnológicas y Desarrollo Nuclear (CEADEN), Cubaenergía, Cuba and Centro de Investigaciones Energéticas, Medioambientales y Tecnológicas (CIEMAT), Spain; Swedish Research Council (VR) and Knut & Alice Wallenberg Foundation (KAW), Sweden; European Organization for Nuclear Research, Switzerland; National Science and Technology Development Agency (NSDTA), Suranaree University of Technology (SUT) and Office of the Higher Education Commission under NRU project of Thailand, Thailand; Turkish Atomic Energy Agency (TAEK), Turkey; National Academy of Sciences of Ukraine, Ukraine; Science and Technology Facilities Council (STFC), United Kingdom; National Science Foundation of the United States of America (NSF) and United States Department of Energy, Office of Nuclear Physics (DOE NP), United States of America.

References

[1] B. Muller, J. Schukraft, B. Wyslouch, First Results from Pb + Pb collisions at the LHC, Annu. Rev. Nucl. Part. Sci. 62 (2012) 361–386, arXiv:1202.3233 [hep-ex].

[2] U. Heinz, R. Snellings, Collective flow and viscosity in relativistic heavy-ion collisions, Annu. Rev. Nucl. Part. Sci. 63 (2013) 123–151, arXiv:1301.2826 [nucl-th].

[3] K.M. Burke, A. Buzzatti, N. Chang, C. Gale, M. Gyulassy, et al., Extracting jet transport coefficient from jet quenching at RHIC and LHC, Phys. Rev. C 90 (2014) 014909, arXiv:1312.5003 [nucl-th].

[4] ALICE Collaboration, B. Abelev, et al., Measurement of the inclusive differential jet cross section in pp collisions at $\sqrt{s} = 2.76$ TeV, Phys. Lett. B 722 (2013) 262–272, arXiv:1301.3475 [nucl-ex].

[5] ATLAS Collaboration, G. Aad, et al., Measurement of the inclusive jet cross-section in proton–proton collisions at $\sqrt{s} = 7$ TeV using 4.5 fb^{-1} of data with the ATLAS detector, J. High Energy Phys. 02 (2015) 153, arXiv:1410.8857 [hep-ex], Erratum: J. High Energy Phys. 09 (2015) 141.

[6] CMS Collaboration, V. Khachatryan, et al., Measurement and QCD analysis of double-differential inclusive jet cross-sections in pp collisions at $\sqrt{s} = 8$ TeV and ratios to 2.76 and 7 TeV, J. High Energy Phys. (2016), submitted for publication, arXiv:1609.05331 [hep-ex].

[7] M. Dasgupta, F. Dreyer, G.P. Salam, G. Soyez, Small-radius jets to all orders in QCD, J. High Energy Phys. 04 (2015) 039, arXiv:1411.5182 [hep-ph].

[8] ALICE Collaboration, B. Abelev, et al., Charged jet cross sections and properties in proton–proton collisions at $\sqrt{s} = 7$ TeV, Phys. Rev. D 91 (11) (2015) 112012, arXiv:1411.4969 [nucl-ex].

[9] ALICE Collaboration, J. Adam, et al., Measurement of jet quenching with semi-inclusive hadron-jet distributions in central Pb–Pb collisions at $\sqrt{s_{\rm NN}} = 2.76$ TeV, J. High Energy Phys. 09 (2015) 170, arXiv:1506.03984 [nucl-ex].

[10] PHENIX Collaboration, K. Adcox, et al., Suppression of hadrons with large transverse momentum in central Au + Au collisions at $\sqrt{s_{\rm NN}} = 130$-GeV, Phys. Rev. Lett. 88 (2002) 022301, arXiv:nucl-ex/0109003.

[11] PHENIX Collaboration, A. Adare, et al., Neutral pion production with respect to centrality and reaction plane in Au + Au collisions at $\sqrt{s_{\rm NN}} = 200$ GeV, Phys. Rev. C 87 (2013) 034911, arXiv:1208.2254 [nucl-ex].

[12] PHENIX Collaboration, A. Adare, et al., Trends in yield and azimuthal shape modification in dihadron correlations in relativistic heavy ion collisions, Phys. Rev. Lett. 104 (2010) 252301, arXiv:1002.1077 [nucl-ex].

[13] PHENIX Collaboration, A. Adare, et al., Medium modification of jet fragmentation in Au + Au collisions at $\sqrt{s_{\rm NN}} = 200$ GeV measured in direct photon–hadron correlations, Phys. Rev. Lett. 111 (2013) 032301, arXiv:1212.3323 [nucl-ex].

[14] STAR Collaboration, C. Adler, et al., Centrality dependence of high $p_{\rm T}$ hadron suppression in Au + Au collisions at $\sqrt{s_{\rm NN}} = 130$-GeV, Phys. Rev. Lett. 89 (2002) 202301, arXiv:nucl-ex/0206011.

[15] STAR Collaboration, C. Adler, et al., Disappearance of back-to-back high $p_{\rm T}$ hadron correlations in central Au + Au collisions at $\sqrt{s_{\rm NN}} = 200$ GeV, Phys. Rev. Lett. 90 (2003) 082302, arXiv:nucl-ex/0210033.

[16] STAR Collaboration, J. Adams, et al., Transverse-momentum and collision-energy dependence of high-$p_{\rm T}$ hadron suppression in Au + Au collisions at ultrarelativistic energies, Phys. Rev. Lett. 91 (2003) 172302, arXiv:nucl-ex/0305015.

[17] STAR Collaboration, J. Adams, et al., Direct observation of dijets in central Au + Au collisions at $\sqrt{s_{\rm NN}} = 200$ GeV, Phys. Rev. Lett. 97 (2006) 162301, arXiv:nucl-ex/0604018.

[18] STAR Collaboration, L. Adamczyk, et al., Jet-hadron correlations in $\sqrt{s_{\rm NN}} = 200$ GeV p + p and central Au + Au collisions, Phys. Rev. Lett. 112 (2014) 122301, arXiv:1302.6184 [nucl-ex].

[19] STAR Collaboration, L. Adamczyk, et al., Di-jet imbalance measurements at $\sqrt{s_{\rm NN}} = 200$ GeV at STAR, Phys. Rev. Lett. 119 (6) (2017) 062301, arXiv:1609.03878 [nucl-ex].

[20] STAR Collaboration, L. Adamczyk, et al., Measurements of jet quenching with semi-inclusive hadron+jet distributions in Au + Au collisions at $\sqrt{s_{\rm NN}} = 200$ GeV, Phys. Rev. C 96 (2) (2017) 024905, arXiv:1702.01108 [nucl-ex].

[21] ALICE Collaboration, K. Aamodt, et al., Particle-yield modification in jet-like azimuthal di-hadron correlations in Pb–Pb collisions at $\sqrt{s_{\rm NN}} = 2.76$ TeV, Phys. Rev. Lett. 108 (2012) 092301, arXiv:1110.0121 [nucl-ex].

[22] ALICE Collaboration, B. Abelev, et al., Centrality dependence of charged particle production at large transverse momentum in Pb–Pb collisions at $\sqrt{s_{\rm NN}} = 2.76$ TeV, Phys. Lett. B 720 (2013) 52–62, arXiv:1208.2711 [hep-ex].

[23] ALICE Collaboration, B. Abelev, et al., Measurement of charged jet suppression in Pb–Pb collisions at $\sqrt{s_{\rm NN}} = 2.76$ TeV, J. High Energy Phys. 03 (2014) 013, arXiv:1311.0633 [nucl-ex].

[24] ALICE Collaboration, J. Adam, et al., Measurement of jet suppression in central Pb–Pb collisions at $\sqrt{s_{\rm NN}} = 2.76$ TeV, Phys. Lett. B 746 (2015) 1–14, arXiv:1502.01689 [nucl-ex].

[25] ALICE Collaboration, J. Adam, et al., Jet-like correlations with neutral pion triggers in pp and central Pb–Pb collisions at 2.76 TeV, Phys. Lett. B 763 (2016) 238–250, arXiv:1608.07201 [nucl-ex].

[26] ATLAS Collaboration, G. Aad, et al., Observation of a centrality-dependent dijet asymmetry in lead–lead collisions at $\sqrt{s_{\rm NN}} = 2.76$ TeV with the ATLAS detector at the LHC, Phys. Rev. Lett. 105 (2010) 252303, arXiv:1011.6182 [hep-ex].

[27] ATLAS Collaboration, G. Aad, et al., Measurements of the nuclear modification factor for jets in Pb + Pb collisions at $\sqrt{s_{\rm NN}} = 2.76$ TeV with the ATLAS detector, Phys. Rev. Lett. 114 (7) (2015) 072302, arXiv:1411.2357 [hep-ex].

[28] CMS Collaboration, S. Chatrchyan, et al., Study of high-$p_{\rm T}$ charged particle suppression in PbPb compared to pp collisions at $\sqrt{s_{\rm NN}} = 2.76$ TeV, Eur. Phys. J. C 72 (2012) 1945, arXiv:1202.2554 [nucl-ex].

[29] CMS Collaboration, S. Chatrchyan, et al., Centrality dependence of dihadron correlations and azimuthal anisotropy harmonics in PbPb collisions at $\sqrt{s_{\rm NN}} = 2.76$ TeV, Eur. Phys. J. C 72 (2012) 10052, arXiv:1201.3158 [nucl-ex].

[30] CMS Collaboration, S. Chatrchyan, et al., Jet momentum dependence of jet quenching in PbPb collisions at $\sqrt{s_{\rm NN}} = 2.76$ TeV, Phys. Lett. B 712 (2012) 176–197, arXiv:1202.5022 [nucl-ex].

[31] CMS Collaboration, S. Chatrchyan, et al., Studies of jet quenching using isolated-photon+jet correlations in PbPb and pp collisions at $\sqrt{s_{\rm NN}} = 2.76$ TeV, Phys. Lett. B 718 (2013) 773–794, arXiv:1205.0206 [nucl-ex].

[32] CMS Collaboration, V. Khachatryan, et al., Measurement of inclusive jet cross-sections in pp and PbPb collisions at $\sqrt{s_{\rm NN}} = 2.76$ TeV, Phys. Rev. C (2016), submitted for publication, arXiv:1609.05383 [nucl-ex].

[33] ALICE Collaboration, B. Abelev, et al., Long-range angular correlations on the near and away side in p–Pb collisions at $\sqrt{s_{\rm NN}} = 5.02$ TeV, Phys. Lett. B 719 (2013) 29–41, arXiv:1212.2001 [nucl-ex].

[34] ALICE Collaboration, B. Abelev, et al., Long-range angular correlations of π, K and p in p–Pb collisions at $\sqrt{s_{\rm NN}} = 5.02$ TeV, Phys. Lett. B 726 (2013) 164–177, arXiv:1307.3237 [nucl-ex].

[35] ALICE Collaboration, B. Abelev, et al., Multiparticle azimuthal correlations in p–Pb and Pb–Pb collisions at the CERN Large Hadron Collider, Phys. Rev. C 90 (5) (2014) 054901, arXiv:1406.2474 [nucl-ex].

[36] ALICE Collaboration, J. Adam, et al., Forward-central two-particle correlations in p–Pb collisions at $\sqrt{s_{\rm NN}} = 5.02$ TeV, Phys. Lett. B 753 (2016) 126–139, arXiv:1506.08032 [nucl-ex].

[37] ATLAS Collaboration, G. Aad, et al., Observation of associated near-side and away-side long-range correlations in $\sqrt{s_{\rm NN}} = 5.02$ TeV proton–lead collisions with the ATLAS detector, Phys. Rev. Lett. 110 (18) (2013) 182302, arXiv:1212.5198 [hep-ex].

[38] ATLAS Collaboration, G. Aad, et al., Measurement with the ATLAS detector of multi-particle azimuthal correlations in p + Pb collisions at $\sqrt{s_{\rm NN}} = 5.02$ TeV, Phys. Lett. B 725 (2013) 60–78, arXiv:1303.2084 [hep-ex].

[39] ATLAS Collaboration, G. Aad, et al., Measurement of long-range pseudorapidity correlations and azimuthal harmonics in $\sqrt{s_{\rm NN}} = 5.02$ TeV proton–lead collisions with the ATLAS detector, Phys. Rev. C 90 (4) (2014) 044906, arXiv:1409.1792 [hep-ex].

[40] CMS Collaboration, V. Khachatryan, et al., Observation of long-range near-side angular correlations in proton–proton collisions at the LHC, J. High Energy Phys. 09 (2010) 091, arXiv:1009.4122 [hep-ex].

[41] CMS Collaboration, S. Chatrchyan, et al., Multiplicity and transverse momentum dependence of two- and four-particle correlations in pPb and PbPb collisions, Phys. Lett. B 724 (2013) 213–240, arXiv:1305.0609 [nucl-ex].

[42] CMS Collaboration, S. Chatrchyan, et al., Long-range angular correlations on the near and away side in p–Pb collisions at $\sqrt{s_{\rm NN}} = 5.02$ TeV, Phys. Lett. B 718 (2013) 795, arXiv:1210.5482 [nucl-ex].

[43] CMS Collaboration, V. Khachatryan, et al., Long-range two-particle correlations of strange hadrons with charged particles in pPb and PbPb collisions at LHC energies, Phys. Lett. B 742 (2015) 200–224, arXiv:1409.3392 [nucl-ex].

[44] CMS Collaboration, S. Khachatryan, et al., Evidence for collective multiparticle correlations in p–Pb collisions, Phys. Rev. Lett. 115 (2015) 012301, arXiv:1502.05382 [nucl-ex].

[45] PHENIX Collaboration, A. Adare, et al., Quadrupole anisotropy in dihadron azimuthal correlations in central d + Au collisions at $\sqrt{s_{\rm NN}} = 200$ GeV, Phys. Rev. Lett. 111 (21) (2013) 212301, arXiv:1303.1794 [nucl-ex].

[46] PHENIX Collaboration, A. Adare, et al., Measurement of long-range angular correlation and quadrupole anisotropy of pions and (anti)protons in central d + Au collisions at $\sqrt{s_{\rm NN}} = 200$ GeV, Phys. Rev. Lett. 114 (19) (2015) 192301, arXiv:1404.7461 [nucl-ex].

[47] PHENIX Collaboration, A. Adare, et al., Measurements of elliptic and triangular flow in high-multiplicity ^{3}He + Au collisions at $\sqrt{s_{\rm NN}} = 200$ GeV, Phys. Rev. Lett. 115 (14) (2015) 142301, arXiv:1507.06273 [nucl-ex].

[48] PHENIX Collaboration, C. Aidala, et al., Measurement of long-range angular correlations and azimuthal anisotropies in high-multiplicity p + Au collisions at $\sqrt{s_{\rm NN}} = 200$ GeV, Phys. Rev. C 95 (3) (2017) 034910, arXiv:1609.02894 [nucl-ex].

[49] STAR Collaboration, L. Adamczyk, et al., Effect of event selection on jetlike correlation measurement in d + Au collisions at $\sqrt{s_{\rm NN}} = 200$ GeV, Phys. Lett. B 743 (2015) 333–339, arXiv:1412.8437 [nucl-ex].

[50] STAR Collaboration, L. Adamczyk, et al., Long-range pseudorapidity dihadron correlations in d + Au collisions at $\sqrt{s_{\rm NN}} = 200$ GeV, Phys. Lett. B 747 (2015) 265–271, arXiv:1502.07652 [nucl-ex].

[51] C.A. Salgado, J.P. Wessels, Proton–lead collisions at the CERN LHC, Annu. Rev. Nucl. Part. Sci. 66 (2016) 449–473.

[52] K. Tywoniuk, Is there jet quenching in pPb? Nucl. Phys. A 926 (2014) 85–91.

[53] B.G. Zakharov, Parton energy loss in the mini quark–gluon plasma and jet quenching in proton–proton collisions, J. Phys. G 41 (2014) 075008, arXiv:1311.1159 [hep-ph].

[54] S.-Y. Chen, K.-M. Shen, W. Dai, B.-W. Zhang, H.-Z. Zhang, E.-K. Wang, Centrality dependence of productions for single hadrons and inclusive jets in high-energy p + A collisions with NLO QCD, Commun. Theor. Phys. 64 (1) (2015) 95–102.

[55] Z.-B. Kang, I. Vitev, H. Xing, Effects of cold nuclear matter energy loss on inclusive jet production in p + A collisions at energies available at the BNL Relativistic Heavy Ion Collider and the CERN Large Hadron Collider, Phys. Rev. C 92 (5) (2015) 054911, arXiv:1507.05987 [hep-ph].

[56] ALICE Collaboration, J. Adam, et al., Centrality dependence of particle production in p–Pb collisions at $\sqrt{s_{\rm NN}} = 5.02$ TeV, Phys. Rev. C 91 (2015) 064905, arXiv:1412.6828 [nucl-ex].

[57] STAR Collaboration, J. Adams, et al., Evidence from d + Au measurements for final state suppression of high-$p_{\rm T}$ hadrons in Au + Au collisions at RHIC, Phys. Rev. Lett. 91 (2003) 072304, arXiv:nucl-ex/0306024.

[58] PHENIX Collaboration, S.S. Adler, et al., Centrality dependence of π^0 and η production at large transverse momentum in $\sqrt{s_{\rm NN}} = 200$ GeV d + Au collisions, Phys. Rev. Lett. 98 (2007) 172302, arXiv:nucl-ex/0610036.

[59] PHENIX Collaboration, A. Adare, et al., Centrality-dependent modification of jet-production rates in deuteron-gold collisions at $\sqrt{s_{\rm NN}} = 200$ GeV, Phys. Rev. Lett. 116 (2016) 122301, arXiv:1509.04657 [nucl-ex].

[60] ATLAS Collaboration, G. Aad, et al., Transverse momentum, rapidity, and centrality dependence of inclusive charged-particle production in $\sqrt{s_{\rm NN}} = 5.02$ TeV p + Pb collisions measured by the ATLAS experiment, Phys. Lett. B 763 (2016) 313–336, arXiv:1605.06436 [hep-ex].

[61] CMS Collaboration, S. Chatrchyan, et al., Studies of dijet transverse momentum balance and pseudorapidity distributions in pPb collisions at $\sqrt{s_{\rm NN}} = 5.02$ TeV, Eur. Phys. J. C 74 (7) (2014) 2951, arXiv:1401.4433 [nucl-ex].

[62] ALICE Collaboration, B. Abelev, et al., Transverse momentum distribution and nuclear modification factor of charged particles in p–Pb collisions at $\sqrt{s_{\rm NN}} = 5.02$ TeV, Phys. Rev. Lett. 110 (2013) 082302, arXiv:1210.4520 [nucl-ex].

[63] CMS Collaboration, V. Khachatryan, et al., Nuclear effects on the transverse momentum spectra of charged particles in pPb collisions at $\sqrt{s_{\rm NN}} = 5.02$ TeV, Eur. Phys. J. C 75 (5) (2015) 237, arXiv:1502.05387 [nucl-ex].

[64] CMS Collaboration, V. Khachatryan, et al., Charged-particle nuclear modification factors in PbPb and pPb collisions at $\sqrt{s_{\rm NN}} = 5.02$ TeV, J. High Energy Phys. 04 (2017) 039, arXiv:1611.01664 [nucl-ex].

[65] ALICE Collaboration, J. Adam, et al., Measurement of charged jet production cross sections and nuclear modification in p–Pb collisions at $\sqrt{s_{\rm NN}} = 5.02$ TeV, Phys. Lett. B 749 (2015) 68–81, arXiv:1503.00681 [nucl-ex].

[66] ATLAS Collaboration, G. Aad, et al., Centrality and rapidity dependence of inclusive jet production in $\sqrt{s_{\rm NN}} = 5.02$ TeV proton–lead collisions with the ATLAS detector, Phys. Lett. B 748 (2015) 392–413, arXiv:1412.4092 [nucl-ex].

[67] CMS Collaboration, V. Khachatryan, et al., Measurement of inclusive jet production and nuclear modifications in pPb collisions at $\sqrt{s_{\rm NN}} = 5.02$ TeV, Eur. Phys. J. C 76 (7) (2016) 372, arXiv:1601.02001 [nucl-ex].

[68] ALICE Collaboration, J. Adam, et al., Centrality dependence of charged jet production in p–Pb collisions at $\sqrt{s_{\rm NN}} = 5.02$ TeV, Eur. Phys. J. C 76 (2016) 271, arXiv:1603.03402 [nucl-ex].

[69] M.L. Miller, K. Reygers, S.J. Sanders, P. Steinberg, Glauber modeling in high energy nuclear collisions, Annu. Rev. Nucl. Part. Sci. 57 (2007) 205–243, arXiv:nucl-ex/0701025.

[70] PHENIX Collaboration, A. Adare, et al., Centrality categorization for $R_{p(d)+A}$ in high-energy collisions, Phys. Rev. C 90 (3) (2014) 034902, arXiv:1310.4793 [nucl-ex].

[71] M. Kordell, A. Majumder, Jets in d(p)–A collisions: color transparency or energy conservation, Phys. Rev. C 97 (5) (2018) 054904, arXiv:1601.02595 [nucl-th], 2016.

[72] D.V. Perepelitsa, P.A. Steinberg, Calculation of centrality bias factors in p + A collisions based on a positive correlation of hard process yields with underlying event activity, arXiv:1412.0976 [nucl-ex].

[73] A. Bzdak, V. Skokov, S. Bathe, Centrality dependence of high energy jets in p + Pb collisions at energies available at the CERN Large Hadron Collider, Phys. Rev. C 93 (4) (2016) 044901, arXiv:1408.3156 [hep-ph].

[74] N. Armesto, D.C. Gülhan, J.G. Milhano, Kinematic bias on centrality selection of jet events in pPb collisions at the LHC, Phys. Lett. B 747 (2015) 441–445, arXiv:1502.02986 [hep-ph].

[75] B.G. Zakharov, Effect of meson cloud on the jet nuclear modification factor in pA collisions, JETP Lett. 105 (2017) 219–222, arXiv:1612.03337 [nucl-th].

[76] M. Alvioli, M. Strikman, Color fluctuation effects in proton–nucleus collisions, Phys. Lett. B 722 (2013) 347–354, arXiv:1301.0728 [hep-ph].

[77] M. Alvioli, L. Frankfurt, V. Guzey, M. Strikman, Revealing "flickering" of the interaction strength in pA collisions at the CERN LHC, Phys. Rev. C 90 (2014) 034914, arXiv:1402.2868 [hep-ph].

[78] M. Alvioli, B.A. Cole, L. Frankfurt, D.V. Perepelitsa, M. Strikman, Evidence for x-dependent proton color fluctuations in pA collisions at the CERN Large Hadron Collider, Phys. Rev. C 93 (1) (2016) 011902, arXiv:1409.7381 [hep-ph].

[79] D. McGlinchey, J.L. Nagle, D.V. Perepelitsa, Consequences of high-x proton size fluctuations in small collision systems at $\sqrt{s_{\rm NN}} = 200$ GeV, Phys. Rev. C 94 (2) (2016) 024915, arXiv:1603.06607 [nucl-th].

[80] C. Loizides, A. Morsch, Absence of jet quenching in peripheral nucleus–nucleus collisions, Phys. Lett. B 773 (2017) 408–411, arXiv:1705.08856 [nucl-ex].

[81] ALICE Collaboration, J. Adam, et al., Measurement of dijet k_T in p–Pb collisions at $\sqrt{s_{NN}} = 5.02$ TeV, Phys. Lett. B 746 (2015) 385–395, arXiv:1503.03050 [nucl-ex].
[82] D. de Florian, Next-to-leading order QCD corrections to hadron+jet production in pp collisions at RHIC, Phys. Rev. D 79 (2009) 114014, arXiv:0904.4402 [hep-ph].
[83] M. Cacciari, G.P. Salam, G. Soyez, The anti-k_t jet clustering algorithm, J. High Energy Phys. 04 (2008) 063, arXiv:0802.1189 [hep-ph].
[84] ALICE Collaboration, K. Aamodt, et al., The ALICE experiment at the CERN LHC, J. Instrum. 3 (2008) S08002.
[85] ALICE Collaboration, B. Abelev, et al., Performance of the ALICE experiment at the CERN LHC, Int. J. Mod. Phys. A 29 (2014) 1430044, arXiv:1402.4476 [nucl-ex].
[86] ALICE Collaboration, B. Abelev, et al., Pseudorapidity density of charged particles in p–Pb collisions at $\sqrt{s_{NN}} = 5.02$ TeV, Phys. Rev. Lett. 110 (2013) 032301.
[87] P.Z. Skands, Tuning Monte Carlo generators: the Perugia tunes, Phys. Rev. D 82 (2010) 074018, arXiv:1005.3457 [hep-ph].
[88] The ALICE definition of primary particles, https://cds.cern.ch/record/2270008?ln=en.
[89] R. Brun, F. Bruyant, M. Maire, A.C. McPherson, P. Zanarini, GEANT3 User's Guide, 1985, CERN Data Handling Division DD/EE/84-1.
[90] T. Sjöstrand, S. Mrenna, P.Z. Skands, A brief introduction to PYTHIA 8.1, Comput. Phys. Commun. 178 (2008) 852–867, arXiv:0710.3820 [hep-ph].
[91] D. d'Enterria, K.J. Eskola, I. Helenius, H. Paukkunen, Confronting current NLO parton fragmentation functions with inclusive charged-particle spectra at hadron colliders, Nucl. Phys. B 883 (2014) 615–628, arXiv:1311.1415 [hep-ph].
[92] D. de Florian, R. Sassot, M. Epele, R.J. Hernández-Pinto, M. Stratmann, Parton-to-pion fragmentation reloaded, Phys. Rev. D 91 (1) (2015) 014035, arXiv:1410.6027 [hep-ph].
[93] M. Cacciari, G.P. Salam, G. Soyez, FastJet user manual, Eur. Phys. J. C 72 (2012) 1896, arXiv:1111.6097 [hep-ph].
[94] M. Cacciari, G.P. Salam, G. Soyez, The catchment area of jets, J. High Energy Phys. 04 (2008) 005, arXiv:0802.1188 [hep-ph].
[95] M. Cacciari, G.P. Salam, Pileup subtraction using jet areas, Phys. Lett. B 659 (2008) 119–126, arXiv:0707.1378 [hep-ph].
[96] CMS Collaboration, S. Chatrchyan, et al., Measurement of the underlying event activity in pp collisions at $\sqrt{s} = 0.9$ and 7 TeV with the novel jet-area/median approach, J. High Energy Phys. 08 (2012) 130, arXiv:1207.2392 [nucl-ex].
[97] R. Baier, Jet quenching, Nucl. Phys. A 715 (2003) 209–218, arXiv:hep-ph/0209038.
[98] A. Drees, H. Feng, J. Jia, Medium induced jet absorption at RHIC, Phys. Rev. C 71 (2005) 034909, arXiv:nucl-th/0310044.
[99] A. Dainese, C. Loizides, G. Paic, Leading-particle suppression in high energy nucleus–nucleus collisions, Eur. Phys. J. C 38 (2005) 461–474, arXiv:hep-ph/0406201.
[100] K. Eskola, H. Honkanen, C. Salgado, U. Wiedemann, The fragility of high-p_T hadron spectra as a hard probe, Nucl. Phys. A 747 (2005) 511–529, arXiv:hep-ph/0406319.
[101] T. Renk, Through the blackness — high-p_T hadrons probing the central region of 200 AGeV Au–Au collisions, Phys. Rev. C 74 (2006) 024903, arXiv:hep-ph/0602045.
[102] C. Loizides, High transverse momentum suppression and surface effects in Cu + Cu and Au + Au collisions within the PQM model, Eur. Phys. J. C 49 (2007) 339–345, arXiv:hep-ph/0608133.
[103] H. Zhang, J. Owens, E. Wang, X.-N. Wang, Dihadron tomography of high-energy nuclear collisions in NLO pQCD, Phys. Rev. Lett. 98 (2007) 212301, arXiv:nucl-th/0701045.
[104] T. Renk, Energy dependence of the dijet imbalance in Pb–Pb collisions at 2.76 ATeV, Phys. Rev. C 86 (2012) 061901, arXiv:1204.5572 [hep-ph].
[105] B. Nachman, M.L. Mangano, Observables for possible QGP signatures in central pp collisions, Eur. Phys. J. C 78 (4) (2018) 343, arXiv:1708.08369 [hep-ph].
[106] ALICE Collaboration, Supplemental material: constraints on jet quenching in p–Pb collisions at $\sqrt{s_{NN}} = 5.02$ TeV measured by the event-activity dependence of semi-inclusive hadron-jet distributions, CERN-PH-EP-2017-012, https://cds.cern.ch/record/2297486.
[107] G. Cowan, A survey of unfolding methods for particle physics, Conf. Proc. C0203181 (2002) 248–257.
[108] A. Höcker, V. Kartvelishvili, SVD approach to data unfolding, Nucl. Instrum. Methods A372 (1996) 469–481, arXiv:hep-ph/9509307.
[109] G. D'Agostini, A multidimensional unfolding method based on Bayes' theorem, Nucl. Instrum. Methods A362 (1995) 487–498.
[110] T. Adye, Unfolding algorithms and tests using RooUnfold, in: CERN-2011-006, 2011, pp. 313–318.
[111] Z.-B. Kang, I. Vitev, H. Xing, Nuclear modification of high transverse momentum particle production in p + A collisions at RHIC and LHC, Phys. Lett. B 718 (2012) 482–487, arXiv:1209.6030 [hep-ph].

ALICE Collaboration

S. Acharya [136], D. Adamová [92], J. Adolfsson [33], M.M. Aggarwal [97], G. Aglieri Rinella [34], M. Agnello [30], N. Agrawal [46], Z. Ahammed [136], S.U. Ahn [76], S. Aiola [141], A. Akindinov [62], M. Al-Turany [104], S.N. Alam [136], D.S.D. Albuquerque [121], D. Aleksandrov [87], B. Alessandro [56], R. Alfaro Molina [71], Y. Ali [15], A. Alici [11,26,51], A. Alkin [3], J. Alme [21], T. Alt [68], L. Altenkamper [21], I. Altsybeev [135], C. Andrei [84], D. Andreou [34], H.A. Andrews [108], A. Andronic [104], M. Angeletti [34], V. Anguelov [102], C. Anson [95], T. Antičić [105], F. Antinori [54], P. Antonioli [51], N. Apadula [79], L. Aphecetche [112], H. Appelshäuser [68], S. Arcelli [26], R. Arnaldi [56], O.W. Arnold [103,116], I.C. Arsene [20], M. Arslandok [102], B. Audurier [112], A. Augustinus [34], R. Averbeck [104], M.D. Azmi [16], A. Badalà [53], Y.W. Baek [75,58], S. Bagnasco [56], R. Bailhache [68], R. Bala [99], A. Baldisseri [72], M. Ball [43], R.C. Baral [65,85], A.M. Barbano [25], R. Barbera [27], F. Barile [32], L. Barioglio [25], G.G. Barnaföldi [140], L.S. Barnby [91], V. Barret [130], P. Bartalini [7], K. Barth [34], E. Bartsch [68], N. Bastid [130], S. Basu [138], G. Batigne [112], B. Batyunya [74], P.C. Batzing [20], J.L. Bazo Alba [109], I.G. Bearden [88], H. Beck [102], C. Bedda [61], N.K. Behera [58], I. Belikov [132], F. Bellini [34,26], H. Bello Martinez [2], R. Bellwied [123], L.G.E. Beltran [119], V. Belyaev [90], G. Bencedi [140], S. Beole [25], A. Bercuci [84], Y. Berdnikov [94], D. Berenyi [140], R.A. Bertens [126], D. Berzano [56,34], L. Betev [34], P.P. Bhaduri [136], A. Bhasin [99], I.R. Bhat [99], B. Bhattacharjee [42], J. Bhom [117], A. Bianchi [25], L. Bianchi [123], N. Bianchi [49], C. Bianchin [138], J. Bielčík [37], J. Bielčíková [92], A. Bilandzic [116,103], G. Biro [140], R. Biswas [4], S. Biswas [4], J.T. Blair [118], D. Blau [87], C. Blume [68], G. Boca [133], F. Bock [34], A. Bogdanov [90], L. Boldizsár [140], M. Bombara [38], G. Bonomi [134], M. Bonora [34], H. Borel [72], A. Borissov [18,102], M. Borri [125], E. Botta [25], C. Bourjau [88], L. Bratrud [68], P. Braun-Munzinger [104], M. Bregant [120], T.A. Broker [68], M. Broz [37], E.J. Brucken [44], E. Bruna [56], G.E. Bruno [34,32], D. Budnikov [106], H. Buesching [68], S. Bufalino [30], P. Buhler [111], P. Buncic [34], O. Busch [129], Z. Buthelezi [73], J.B. Butt [15], J.T. Buxton [17], J. Cabala [114], D. Caffarri [34,89], H. Caines [141], A. Caliva [104,61], E. Calvo Villar [109], R.S. Camacho [2], P. Camerini [24], A.A. Capon [111], F. Carena [34], W. Carena [34], F. Carnesecchi [11,26], J. Castillo Castellanos [72], A.J. Castro [126], E.A.R. Casula [52], C. Ceballos Sanchez [9], S. Chandra [136], B. Chang [124], W. Chang [7], S. Chapeland [34], M. Chartier [125], S. Chattopadhyay [136], S. Chattopadhyay [107],

A. Chauvin [103,116], C. Cheshkov [131], B. Cheynis [131], V. Chibante Barroso [34], D.D. Chinellato [121], S. Cho [58], P. Chochula [34], M. Chojnacki [88], S. Choudhury [136], T. Chowdhury [130], P. Christakoglou [89], C.H. Christensen [88], P. Christiansen [33], T. Chujo [129], S.U. Chung [18], C. Cicalo [52], L. Cifarelli [11,26], F. Cindolo [51], J. Cleymans [98], F. Colamaria [50,32], D. Colella [63,34,50], A. Collu [79], M. Colocci [26], M. Concas [56,ii], G. Conesa Balbastre [78], Z. Conesa del Valle [59], J.G. Contreras [37], T.M. Cormier [93], Y. Corrales Morales [56], I. Cortés Maldonado [2], P. Cortese [31], M.R. Cosentino [122], F. Costa [34], S. Costanza [133], J. Crkovská [59], P. Crochet [130], E. Cuautle [69], L. Cunqueiro [139,93], T. Dahms [116,103], A. Dainese [54], M.C. Danisch [102], A. Danu [66], D. Das [107], I. Das [107], S. Das [4], A. Dash [85], S. Dash [46], S. De [47], A. De Caro [29], G. de Cataldo [50], C. de Conti [120], J. de Cuveland [40], A. De Falco [23], D. De Gruttola [11,29], N. De Marco [56], S. De Pasquale [29], R.D. De Souza [121], H.F. Degenhardt [120], A. Deisting [104,102], A. Deloff [83], S. Delsanto [25], C. Deplano [89], P. Dhankher [46], D. Di Bari [32], A. Di Mauro [34], P. Di Nezza [49], B. Di Ruzza [54], T. Dietel [98], P. Dillenseger [68], Y. Ding [7], R. Divià [34], Ø. Djuvsland [21], A. Dobrin [34], D. Domenicis Gimenez [120], B. Dönigus [68], O. Dordic [20], L.V.R. Doremalen [61], A.K. Dubey [136], A. Dubla [104], L. Ducroux [131], S. Dudi [97], A.K. Duggal [97], M. Dukhishyam [85], P. Dupieux [130], R.J. Ehlers [141], D. Elia [50], E. Endress [109], H. Engel [67], E. Epple [141], B. Erazmus [112], F. Erhardt [96], B. Espagnon [59], G. Eulisse [34], J. Eum [18], D. Evans [108], S. Evdokimov [110], L. Fabbietti [103,116], J. Faivre [78], A. Fantoni [49], M. Fasel [93], L. Feldkamp [139], A. Feliciello [56], G. Feofilov [135], A. Fernández Téllez [2], A. Ferretti [25], A. Festanti [28,34], V.J.G. Feuillard [72,130], J. Figiel [117], M.A.S. Figueredo [120], S. Filchagin [106], D. Finogeev [60], F.M. Fionda [21,23], M. Floris [34], S. Foertsch [73], P. Foka [104], S. Fokin [87], E. Fragiacomo [57], A. Francescon [34], A. Francisco [112], U. Frankenfeld [104], G.G. Fronze [25], U. Fuchs [34], C. Furget [78], A. Furs [60], M. Fusco Girard [29], J.J. Gaardhøje [88], M. Gagliardi [25], A.M. Gago [109], K. Gajdosova [88], M. Gallio [25], C.D. Galvan [119], P. Ganoti [82], C. Garabatos [104], E. Garcia-Solis [12], K. Garg [27], C. Gargiulo [34], P. Gasik [103,116], E.F. Gauger [118], M.B. Gay Ducati [70], M. Germain [112], J. Ghosh [107], P. Ghosh [136], S.K. Ghosh [4], P. Gianotti [49], P. Giubellino [34,104,56], P. Giubilato [28], E. Gladysz-Dziadus [117], P. Glässel [102], D.M. Goméz Coral [71], A. Gomez Ramirez [67], A.S. Gonzalez [34], P. González-Zamora [2], S. Gorbunov [40], L. Görlich [117], S. Gotovac [115], V. Grabski [71], L.K. Graczykowski [137], K.L. Graham [108], L. Greiner [79], A. Grelli [61], C. Grigoras [34], V. Grigoriev [90], A. Grigoryan [1], S. Grigoryan [74], J.M. Gronefeld [104], F. Grosa [30], J.F. Grosse-Oetringhaus [34], R. Grosso [104], F. Guber [60], R. Guernane [78], B. Guerzoni [26], M. Guittiere [112], K. Gulbrandsen [88], T. Gunji [128], A. Gupta [99], R. Gupta [99], I.B. Guzman [2], R. Haake [34], C. Hadjidakis [59], H. Hamagaki [80], G. Hamar [140], J.C. Hamon [132], M.R. Haque [61], J.W. Harris [141], A. Harton [12], H. Hassan [78], D. Hatzifotiadou [11,51], S. Hayashi [128], S.T. Heckel [68], E. Hellbär [68], H. Helstrup [35], A. Herghelegiu [84], E.G. Hernandez [2], G. Herrera Corral [10], F. Herrmann [139], B.A. Hess [101], K.F. Hetland [35], H. Hillemanns [34], C. Hills [125], B. Hippolyte [132], B. Hohlweger [103], D. Horak [37], S. Hornung [104], R. Hosokawa [129,78], P. Hristov [34], C. Hughes [126], T.J. Humanic [17], N. Hussain [42], T. Hussain [16], D. Hutter [40], D.S. Hwang [19], J.P. Iddon [125], S.A. Iga Buitron [69], R. Ilkaev [106], M. Inaba [129], M. Ippolitov [90,87], M.S. Islam [107], M. Ivanov [104], V. Ivanov [94], V. Izucheev [110], B. Jacak [79], N. Jacazio [26], P.M. Jacobs [79], M.B. Jadhav [46], S. Jadlovska [114], J. Jadlovsky [114], S. Jaelani [61], C. Jahnke [116], M.J. Jakubowska [137], M.A. Janik [137], P.H.S.Y. Jayarathna [123], C. Jena [85], M. Jercic [96], R.T. Jimenez Bustamante [104], P.G. Jones [108], A. Jusko [108], P. Kalinak [63], A. Kalweit [34], J.H. Kang [142], V. Kaplin [90], S. Kar [136], A. Karasu Uysal [77], O. Karavichev [60], T. Karavicheva [60], L. Karayan [104,102], P. Karczmarczyk [34], E. Karpechev [60], U. Kebschull [67], R. Keidel [143], D.L.D. Keijdener [61], M. Keil [34], B. Ketzer [43], Z. Khabanova [89], P. Khan [107], S. Khan [16], S.A. Khan [136], A. Khanzadeev [94], Y. Kharlov [110], A. Khatun [16], A. Khuntia [47], M.M. Kielbowicz [117], B. Kileng [35], B. Kim [129], D. Kim [142], D.J. Kim [124], E.J. Kim [14], H. Kim [142], J.S. Kim [41], J. Kim [102], M. Kim [58], S. Kim [19], T. Kim [142], S. Kirsch [40], I. Kisel [40], S. Kiselev [62], A. Kisiel [137], G. Kiss [140], J.L. Klay [6], C. Klein [68], J. Klein [34], C. Klein-Bösing [139], S. Klewin [102], A. Kluge [34], M.L. Knichel [102,34], A.G. Knospe [123], C. Kobdaj [113], M. Kofarago [140], M.K. Köhler [102], T. Kollegger [104], V. Kondratiev [135], N. Kondratyeva [90], E. Kondratyuk [110], A. Konevskikh [60], M. Konyushikhin [138], M. Kopcik [114], M. Kour [99], C. Kouzinopoulos [34], O. Kovalenko [83], V. Kovalenko [135], M. Kowalski [117], I. Králik [63], A. Kravčáková [38], L. Kreis [104], M. Krivda [108,63], F. Krizek [92], E. Kryshen [94], M. Krzewicki [40], A.M. Kubera [17], V. Kučera [92], C. Kuhn [132], P.G. Kuijer [89], A. Kumar [99], J. Kumar [46], L. Kumar [97], S. Kumar [46], S. Kundu [85], P. Kurashvili [83], A. Kurepin [60], A.B. Kurepin [60], A. Kuryakin [106], S. Kushpil [92], M.J. Kweon [58], Y. Kwon [142], S.L. La Pointe [40], P. La Rocca [27], C. Lagana Fernandes [120], Y.S. Lai [79], I. Lakomov [34], R. Langoy [39], K. Lapidus [141], C. Lara [67], A. Lardeux [20], A. Lattuca [25], E. Laudi [34],

R. Lavicka [37], R. Lea [24], L. Leardini [102], S. Lee [142], F. Lehas [89], S. Lehner [111], J. Lehrbach [40], R.C. Lemmon [91], E. Leogrande [61], I. León Monzón [119], P. Lévai [140], X. Li [13], X.L. Li [7], J. Lien [39], R. Lietava [108], B. Lim [18], S. Lindal [20], V. Lindenstruth [40], S.W. Lindsay [125], C. Lippmann [104], M.A. Lisa [17], V. Litichevskyi [44], A. Liu [79], W.J. Llope [138], D.F. Lodato [61], P.I. Loenne [21], V. Loginov [90], C. Loizides [79,93], P. Loncar [115], X. Lopez [130], E. López Torres [9], A. Lowe [140], P. Luettig [68], J.R. Luhder [139], M. Lunardon [28], G. Luparello [24,57], M. Lupi [34], T.H. Lutz [141], A. Maevskaya [60], M. Mager [34], S.M. Mahmood [20], A. Maire [132], R.D. Majka [141], M. Malaev [94], L. Malinina [74,iii], D. Mal'Kevich [62], P. Malzacher [104], A. Mamonov [106], V. Manko [87], F. Manso [130], V. Manzari [50], Y. Mao [7], M. Marchisone [131,127,73], J. Mareš [64], G.V. Margagliotti [24], A. Margotti [51], J. Margutti [61], A. Marín [104], C. Markert [118], M. Marquard [68], N.A. Martin [104], P. Martinengo [34], J.A.L. Martinez [67], M.I. Martínez [2], G. Martínez García [112], M. Martinez Pedreira [34], S. Masciocchi [104], M. Masera [25], A. Masoni [52], L. Massacrier [59], E. Masson [112], A. Mastroserio [50], A.M. Mathis [116,103], P.F.T. Matuoka [120], A. Matyja [126], C. Mayer [117], J. Mazer [126], M. Mazzilli [32], M.A. Mazzoni [55], F. Meddi [22], Y. Melikyan [90], A. Menchaca-Rocha [71], E. Meninno [29], J. Mercado Pérez [102], M. Meres [36], S. Mhlanga [98], Y. Miake [129], M.M. Mieskolainen [44], D.L. Mihaylov [103], K. Mikhaylov [62,74], A. Mischke [61], A.N. Mishra [47], D. Miśkowiec [104], J. Mitra [136], C.M. Mitu [66], N. Mohammadi [34,61], A.P. Mohanty [61], B. Mohanty [85], M. Mohisin Khan [16,iv], D.A. Moreira De Godoy [139], L.A.P. Moreno [2], S. Moretto [28], A. Morreale [112], A. Morsch [34], V. Muccifora [49], E. Mudnic [115], D. Mühlheim [139], S. Muhuri [136], M. Mukherjee [4], J.D. Mulligan [141], M.G. Munhoz [120], K. Münning [43], M.I.A. Munoz [79], R.H. Munzer [68], H. Murakami [128], S. Murray [73], L. Musa [34], J. Musinsky [63], C.J. Myers [123], J.W. Myrcha [137], B. Naik [46], R. Nair [83], B.K. Nandi [46], R. Nania [11,51], E. Nappi [50], A. Narayan [46], M.U. Naru [15], H. Natal da Luz [120], C. Nattrass [126], S.R. Navarro [2], K. Nayak [85], R. Nayak [46], T.K. Nayak [136], S. Nazarenko [106], R.A. Negrao De Oliveira [68,34], L. Nellen [69], S.V. Nesbo [35], G. Neskovic [40], F. Ng [123], M. Nicassio [104], M. Niculescu [66], J. Niedziela [137,34], B.S. Nielsen [88], S. Nikolaev [87], S. Nikulin [87], V. Nikulin [94], A. Nobuhiro [45], F. Noferini [11,51], P. Nomokonov [74], G. Nooren [61], J.C.C. Noris [2], J. Norman [125,78], A. Nyanin [87], J. Nystrand [21], H. Oeschler [18,102,i], H. Oh [142], A. Ohlson [102], L. Olah [140], J. Oleniacz [137], A.C. Oliveira Da Silva [120], M.H. Oliver [141], J. Onderwaater [104], C. Oppedisano [56], R. Orava [44], M. Oravec [114], A. Ortiz Velasquez [69], A. Oskarsson [33], J. Otwinowski [117], K. Oyama [80], Y. Pachmayer [102], V. Pacik [88], D. Pagano [134], G. Paić [69], P. Palni [7], J. Pan [138], A.K. Pandey [46], S. Panebianco [72], V. Papikyan [1], P. Pareek [47], J. Park [58], S. Parmar [97], A. Passfeld [139], S.P. Pathak [123], R.N. Patra [136], B. Paul [56], H. Pei [7], T. Peitzmann [61], X. Peng [7], L.G. Pereira [70], H. Pereira Da Costa [72], D. Peresunko [90,87], E. Perez Lezama [68], V. Peskov [68], Y. Pestov [5], V. Petráček [37], M. Petrovici [84], C. Petta [27], R.P. Pezzi [70], S. Piano [57], M. Pikna [36], P. Pillot [112], L.O.D.L. Pimentel [88], O. Pinazza [51,34], L. Pinsky [123], D.B. Piyarathna [123], M. Płoskoń [79], M. Planinic [96], F. Pliquett [68], J. Pluta [137], S. Pochybova [140], P.L.M. Podesta-Lerma [119], M.G. Poghosyan [93], B. Polichtchouk [110], N. Poljak [96], W. Poonsawat [113], A. Pop [84], H. Poppenborg [139], S. Porteboeuf-Houssais [130], V. Pozdniakov [74], S.K. Prasad [4], R. Preghenella [51], F. Prino [56], C.A. Pruneau [138], I. Pshenichnov [60], M. Puccio [25], V. Punin [106], J. Putschke [138], S. Raha [4], S. Rajput [99], J. Rak [124], A. Rakotozafindrabe [72], L. Ramello [31], F. Rami [132], D.B. Rana [123], R. Raniwala [100], S. Raniwala [100], S.S. Räsänen [44], B.T. Rascanu [68], D. Rathee [97], V. Ratza [43], I. Ravasenga [30], K.F. Read [126,93], K. Redlich [83,v], A. Rehman [21], P. Reichelt [68], F. Reidt [34], X. Ren [7], R. Renfordt [68], A. Reshetin [60], K. Reygers [102], V. Riabov [94], T. Richert [61,33], M. Richter [20], P. Riedler [34], W. Riegler [34], F. Riggi [27], C. Ristea [66], M. Rodríguez Cahuantzi [2], K. Røed [20], R. Rogalev [110], E. Rogochaya [74], D. Rohr [34,40], D. Röhrich [21], P.S. Rokita [137], F. Ronchetti [49], E.D. Rosas [69], K. Roslon [137], P. Rosnet [130], A. Rossi [54,28], A. Rotondi [133], F. Roukoutakis [82], C. Roy [132], P. Roy [107], O.V. Rueda [69], R. Rui [24], B. Rumyantsev [74], A. Rustamov [86], E. Ryabinkin [87], Y. Ryabov [94], A. Rybicki [117], S. Saarinen [44], S. Sadhu [136], S. Sadovsky [110], K. Šafařík [34], S.K. Saha [136], B. Sahoo [46], P. Sahoo [47], R. Sahoo [47], S. Sahoo [65], P.K. Sahu [65], J. Saini [136], S. Sakai [129], M.A. Saleh [138], J. Salzwedel [17], S. Sambyal [99], V. Samsonov [94,90], A. Sandoval [71], A. Sarkar [73], D. Sarkar [136], N. Sarkar [136], P. Sarma [42], M.H.P. Sas [61], E. Scapparone [51], F. Scarlassara [28], B. Schaefer [93], H.S. Scheid [68], C. Schiaua [84], R. Schicker [102], C. Schmidt [104], H.R. Schmidt [101], M.O. Schmidt [102], M. Schmidt [101], N.V. Schmidt [93,68], J. Schukraft [34], Y. Schutz [34,132], K. Schwarz [104], K. Schweda [104], G. Scioli [26], E. Scomparin [56], M. Šefčík [38], J.E. Seger [95], Y. Sekiguchi [128], D. Sekihata [45], I. Selyuzhenkov [104,90], K. Senosi [73], S. Senyukov [132], E. Serradilla [71], P. Sett [46], A. Sevcenco [66], A. Shabanov [60], A. Shabetai [112], R. Shahoyan [34], W. Shaikh [107], A. Shangaraev [110], A. Sharma [97], A. Sharma [99], M. Sharma [99], M. Sharma [99], N. Sharma [97], A.I. Sheikh [136], K. Shigaki [45], M. Shimomura [81],

S. Shirinkin [62], Q. Shou [7], K. Shtejer [9,25], Y. Sibiriak [87], S. Siddhanta [52], K.M. Sielewicz [34], T. Siemiarczuk [83], S. Silaeva [87], D. Silvermyr [33], G. Simatovic [89,96], G. Simonetti [34], R. Singaraju [136], R. Singh [85], V. Singhal [136], T. Sinha [107], B. Sitar [36], M. Sitta [31], T.B. Skaali [20], M. Slupecki [124], N. Smirnov [141], R.J.M. Snellings [61], T.W. Snellman [124], J. Song [18], F. Soramel [28], S. Sorensen [126], F. Sozzi [104], I. Sputowska [117], J. Stachel [102], I. Stan [66], P. Stankus [93], E. Stenlund [33], D. Stocco [112], M.M. Storetvedt [35], P. Strmen [36], A.A.P. Suaide [120], T. Sugitate [45], C. Suire [59], M. Suleymanov [15], M. Suljic [24], R. Sultanov [62], M. Šumbera [92], S. Sumowidagdo [48], K. Suzuki [111], S. Swain [65], A. Szabo [36], I. Szarka [36], U. Tabassam [15], J. Takahashi [121], G.J. Tambave [21], N. Tanaka [129], M. Tarhini [112,59], M. Tariq [16], M.G. Tarzila [84], A. Tauro [34], G. Tejeda Muñoz [2], A. Telesca [34], K. Terasaki [128], C. Terrevoli [28], B. Teyssier [131], D. Thakur [47], S. Thakur [136], D. Thomas [118], F. Thoresen [88], R. Tieulent [131], A. Tikhonov [60], A.R. Timmins [123], A. Toia [68], M. Toppi [49], S.R. Torres [119], S. Tripathy [47], S. Trogolo [25], G. Trombetta [32], L. Tropp [38], V. Trubnikov [3], W.H. Trzaska [124], B.A. Trzeciak [61], T. Tsuji [128], A. Tumkin [106], R. Turrisi [54], T.S. Tveter [20], K. Ullaland [21], E.N. Umaka [123], A. Uras [131], G.L. Usai [23], A. Utrobicic [96], M. Vala [114,63], J. Van Der Maarel [61], J.W. Van Hoorne [34], M. van Leeuwen [61], T. Vanat [92], P. Vande Vyvre [34], D. Varga [140], A. Vargas [2], M. Vargyas [124], R. Varma [46], M. Vasileiou [82], A. Vasiliev [87], A. Vauthier [78], O. Vázquez Doce [103,116], V. Vechernin [135], A.M. Veen [61], A. Velure [21], E. Vercellin [25], S. Vergara Limón [2], L. Vermunt [61], R. Vernet [8], R. Vértesi [140], L. Vickovic [115], J. Viinikainen [124], Z. Vilakazi [127], O. Villalobos Baillie [108], A. Villatoro Tello [2], A. Vinogradov [87], L. Vinogradov [135], T. Virgili [29], V. Vislavicius [33], A. Vodopyanov [74], M.A. Völkl [101], K. Voloshin [62], S.A. Voloshin [138], G. Volpe [32], B. von Haller [34], I. Vorobyev [103,116], D. Voscek [114], D. Vranic [34,104], J. Vrláková [38], B. Wagner [21], H. Wang [61], M. Wang [7], Y. Watanabe [128,129], M. Weber [111], S.G. Weber [104], A. Wegrzynek [34], D.F. Weiser [102], S.C. Wenzel [34], J.P. Wessels [139], U. Westerhoff [139], A.M. Whitehead [98], J. Wiechula [68], J. Wikne [20], G. Wilk [83], J. Wilkinson [51], G.A. Willems [139,34], M.C.S. Williams [51], E. Willsher [108], B. Windelband [102], W.E. Witt [126], R. Xu [7], S. Yalcin [77], K. Yamakawa [45], P. Yang [7], S. Yano [45], Z. Yin [7], H. Yokoyama [78,129], I.-K. Yoo [18], J.H. Yoon [58], E. Yun [18], V. Yurchenko [3], V. Zaccolo [56], A. Zaman [15], C. Zampolli [34], H.J.C. Zanoli [120], N. Zardoshti [108], A. Zarochentsev [135], P. Závada [64], N. Zaviyalov [106], H. Zbroszczyk [137], M. Zhalov [94], H. Zhang [7,21], X. Zhang [7], Y. Zhang [7], C. Zhang [61], Z. Zhang [130,7], C. Zhao [20], N. Zhigareva [62], D. Zhou [7], Y. Zhou [88], Z. Zhou [21], H. Zhu [21], J. Zhu [7], Y. Zhu [7], A. Zichichi [26,11], M.B. Zimmermann [34], G. Zinovjev [3], J. Zmeskal [111], S. Zou [7]

[1] *A.I. Alikhanyan National Science Laboratory (Yerevan Physics Institute) Foundation, Yerevan, Armenia*
[2] *Benemérita Universidad Autónoma de Puebla, Puebla, Mexico*
[3] *Bogolyubov Institute for Theoretical Physics, Kiev, Ukraine*
[4] *Bose Institute, Department of Physics and Centre for Astroparticle Physics and Space Science (CAPSS), Kolkata, India*
[5] *Budker Institute for Nuclear Physics, Novosibirsk, Russia*
[6] *California Polytechnic State University, San Luis Obispo, CA, United States*
[7] *Central China Normal University, Wuhan, China*
[8] *Centre de Calcul de l'IN2P3, Villeurbanne, Lyon, France*
[9] *Centro de Aplicaciones Tecnológicas y Desarrollo Nuclear (CEADEN), Havana, Cuba*
[10] *Centro de Investigación y de Estudios Avanzados (CINVESTAV), Mexico City and Mérida, Mexico*
[11] *Centro Fermi – Museo Storico della Fisica e Centro Studi e Ricerche "Enrico Fermi", Rome, Italy*
[12] *Chicago State University, Chicago, IL, United States*
[13] *China Institute of Atomic Energy, Beijing, China*
[14] *Chonbuk National University, Jeonju, Republic of Korea*
[15] *COMSATS Institute of Information Technology (CIIT), Islamabad, Pakistan*
[16] *Department of Physics, Aligarh Muslim University, Aligarh, India*
[17] *Department of Physics, Ohio State University, Columbus, OH, United States*
[18] *Department of Physics, Pusan National University, Pusan, Republic of Korea*
[19] *Department of Physics, Sejong University, Seoul, Republic of Korea*
[20] *Department of Physics, University of Oslo, Oslo, Norway*
[21] *Department of Physics and Technology, University of Bergen, Bergen, Norway*
[22] *Dipartimento di Fisica dell'Università 'La Sapienza' and Sezione INFN, Rome, Italy*
[23] *Dipartimento di Fisica dell'Università and Sezione INFN, Cagliari, Italy*
[24] *Dipartimento di Fisica dell'Università and Sezione INFN, Trieste, Italy*
[25] *Dipartimento di Fisica dell'Università and Sezione INFN, Turin, Italy*
[26] *Dipartimento di Fisica e Astronomia dell'Università and Sezione INFN, Bologna, Italy*
[27] *Dipartimento di Fisica e Astronomia dell'Università and Sezione INFN, Catania, Italy*
[28] *Dipartimento di Fisica e Astronomia dell'Università and Sezione INFN, Padova, Italy*
[29] *Dipartimento di Fisica 'E.R. Caianiello' dell'Università and Gruppo Collegato INFN, Salerno, Italy*
[30] *Dipartimento DISAT del Politecnico and Sezione INFN, Turin, Italy*
[31] *Dipartimento di Scienze e Innovazione Tecnologica dell'Università del Piemonte Orientale and INFN Sezione di Torino, Alessandria, Italy*
[32] *Dipartimento Interateneo di Fisica 'M. Merlin' and Sezione INFN, Bari, Italy*
[33] *Division of Experimental High Energy Physics, University of Lund, Lund, Sweden*
[34] *European Organization for Nuclear Research (CERN), Geneva, Switzerland*
[35] *Faculty of Engineering, Bergen University College, Bergen, Norway*
[36] *Faculty of Mathematics, Physics and Informatics, Comenius University, Bratislava, Slovakia*

[37] Faculty of Nuclear Sciences and Physical Engineering, Czech Technical University in Prague, Prague, Czech Republic
[38] Faculty of Science, P.J. Šafárik University, Košice, Slovakia
[39] Faculty of Technology, Buskerud and Vestfold University College, Tonsberg, Norway
[40] Frankfurt Institute for Advanced Studies, Johann Wolfgang Goethe-Universität Frankfurt, Frankfurt, Germany
[41] Gangneung-Wonju National University, Gangneung, Republic of Korea
[42] Gauhati University, Department of Physics, Guwahati, India
[43] Helmholtz-Institut für Strahlen- und Kernphysik, Rheinische Friedrich-Wilhelms-Universität Bonn, Bonn, Germany
[44] Helsinki Institute of Physics (HIP), Helsinki, Finland
[45] Hiroshima University, Hiroshima, Japan
[46] Indian Institute of Technology Bombay (IIT), Mumbai, India
[47] Indian Institute of Technology Indore, Indore, India
[48] Indonesian Institute of Sciences, Jakarta, Indonesia
[49] INFN, Laboratori Nazionali di Frascati, Frascati, Italy
[50] INFN, Sezione di Bari, Bari, Italy
[51] INFN, Sezione di Bologna, Bologna, Italy
[52] INFN, Sezione di Cagliari, Cagliari, Italy
[53] INFN, Sezione di Catania, Catania, Italy
[54] INFN, Sezione di Padova, Padova, Italy
[55] INFN, Sezione di Roma, Rome, Italy
[56] INFN, Sezione di Torino, Turin, Italy
[57] INFN, Sezione di Trieste, Trieste, Italy
[58] Inha University, Incheon, Republic of Korea
[59] Institut de Physique Nucléaire d'Orsay (IPNO), Université Paris-Sud, CNRS-IN2P3, Orsay, France
[60] Institute for Nuclear Research, Academy of Sciences, Moscow, Russia
[61] Institute for Subatomic Physics of Utrecht University, Utrecht, Netherlands
[62] Institute for Theoretical and Experimental Physics, Moscow, Russia
[63] Institute of Experimental Physics, Slovak Academy of Sciences, Košice, Slovakia
[64] Institute of Physics, Academy of Sciences of the Czech Republic, Prague, Czech Republic
[65] Institute of Physics, Bhubaneswar, India
[66] Institute of Space Science (ISS), Bucharest, Romania
[67] Institut für Informatik, Johann Wolfgang Goethe-Universität Frankfurt, Frankfurt, Germany
[68] Institut für Kernphysik, Johann Wolfgang Goethe-Universität Frankfurt, Frankfurt, Germany
[69] Instituto de Ciencias Nucleares, Universidad Nacional Autónoma de México, Mexico City, Mexico
[70] Instituto de Física, Universidade Federal do Rio Grande do Sul (UFRGS), Porto Alegre, Brazil
[71] Instituto de Física, Universidad Nacional Autónoma de México, Mexico City, Mexico
[72] IRFU, CEA, Université Paris-Saclay, Saclay, France
[73] iThemba LABS, National Research Foundation, Somerset West, South Africa
[74] Joint Institute for Nuclear Research (JINR), Dubna, Russia
[75] Konkuk University, Seoul, Republic of Korea
[76] Korea Institute of Science and Technology Information, Daejeon, Republic of Korea
[77] KTO Karatay University, Konya, Turkey
[78] Laboratoire de Physique Subatomique et de Cosmologie, Université Grenoble-Alpes, CNRS-IN2P3, Grenoble, France
[79] Lawrence Berkeley National Laboratory, Berkeley, CA, United States
[80] Nagasaki Institute of Applied Science, Nagasaki, Japan
[81] Nara Women's University (NWU), Nara, Japan
[82] National and Kapodistrian University of Athens, School of Science, Department of Physics, Athens, Greece
[83] National Centre for Nuclear Studies, Warsaw, Poland
[84] National Institute for Physics and Nuclear Engineering, Bucharest, Romania
[85] National Institute of Science Education and Research, HBNI, Jatni, India
[86] National Nuclear Research Center, Baku, Azerbaijan
[87] National Research Centre Kurchatov Institute, Moscow, Russia
[88] Niels Bohr Institute, University of Copenhagen, Copenhagen, Denmark
[89] Nikhef, Nationaal instituut voor subatomaire fysica, Amsterdam, Netherlands
[90] NRNU Moscow Engineering Physics Institute, Moscow, Russia
[91] Nuclear Physics Group, STFC Daresbury Laboratory, Daresbury, United Kingdom
[92] Nuclear Physics Institute, Academy of Sciences of the Czech Republic, Řež u Prahy, Czech Republic
[93] Oak Ridge National Laboratory, Oak Ridge, TN, United States
[94] Petersburg Nuclear Physics Institute, Gatchina, Russia
[95] Physics Department, Creighton University, Omaha, NE, United States
[96] Physics department, Faculty of science, University of Zagreb, Zagreb, Croatia
[97] Physics Department, Panjab University, Chandigarh, India
[98] Physics Department, University of Cape Town, Cape Town, South Africa
[99] Physics Department, University of Jammu, Jammu, India
[100] Physics Department, University of Rajasthan, Jaipur, India
[101] Physikalisches Institut, Eberhard Karls Universität Tübingen, Tübingen, Germany
[102] Physikalisches Institut, Ruprecht-Karls-Universität Heidelberg, Heidelberg, Germany
[103] Physik Department, Technische Universität München, Munich, Germany
[104] Research Division and ExtreMe Matter Institute EMMI, GSI Helmholtzzentrum für Schwerionenforschung GmbH, Darmstadt, Germany
[105] Rudjer Bošković Institute, Zagreb, Croatia
[106] Russian Federal Nuclear Center (VNIIEF), Sarov, Russia
[107] Saha Institute of Nuclear Physics, Kolkata, India
[108] School of Physics and Astronomy, University of Birmingham, Birmingham, United Kingdom
[109] Sección Física, Departamento de Ciencias, Pontificia Universidad Católica del Perú, Lima, Peru
[110] SSC IHEP of NRC Kurchatov institute, Protvino, Russia
[111] Stefan Meyer Institut für Subatomare Physik (SMI), Vienna, Austria
[112] SUBATECH, IMT Atlantique, Université de Nantes, CNRS-IN2P3, Nantes, France
[113] Suranaree University of Technology, Nakhon Ratchasima, Thailand
[114] Technical University of Košice, Košice, Slovakia
[115] Technical University of Split FESB, Split, Croatia

[116] *Technische Universität München, Excellence Cluster 'Universe', Munich, Germany*
[117] *The Henryk Niewodniczanski Institute of Nuclear Physics, Polish Academy of Sciences, Cracow, Poland*
[118] *The University of Texas at Austin, Austin, TX, United States*
[119] *Universidad Autónoma de Sinaloa, Culiacán, Mexico*
[120] *Universidade de São Paulo (USP), São Paulo, Brazil*
[121] *Universidade Estadual de Campinas (UNICAMP), Campinas, Brazil*
[122] *Universidade Federal do ABC, Santo Andre, Brazil*
[123] *University of Houston, Houston, TX, United States*
[124] *University of Jyväskylä, Jyväskylä, Finland*
[125] *University of Liverpool, Liverpool, United Kingdom*
[126] *University of Tennessee, Knoxville, TN, United States*
[127] *University of the Witwatersrand, Johannesburg, South Africa*
[128] *University of Tokyo, Tokyo, Japan*
[129] *University of Tsukuba, Tsukuba, Japan*
[130] *Université Clermont Auvergne, CNRS/IN2P3, LPC, Clermont-Ferrand, France*
[131] *Université de Lyon, Université Lyon 1, CNRS/IN2P3, IPN-Lyon, Villeurbanne, Lyon, France*
[132] *Université de Strasbourg, CNRS, IPHC UMR 7178, F-67000 Strasbourg, France*
[133] *Università degli Studi di Pavia, Pavia, Italy*
[134] *Università di Brescia, Brescia, Italy*
[135] *V. Fock Institute for Physics, St. Petersburg State University, St. Petersburg, Russia*
[136] *Variable Energy Cyclotron Centre, Kolkata, India*
[137] *Warsaw University of Technology, Warsaw, Poland*
[138] *Wayne State University, Detroit, MI, United States*
[139] *Westfälische Wilhelms-Universität Münster, Institut für Kernphysik, Münster, Germany*
[140] *Wigner Research Centre for Physics, Hungarian Academy of Sciences, Budapest, Hungary*
[141] *Yale University, New Haven, CT, United States*
[142] *Yonsei University, Seoul, Republic of Korea*
[143] *Zentrum für Technologietransfer und Telekommunikation (ZTT), Fachhochschule Worms, Worms, Germany*

[i] Deceased.
[ii] Dipartimento DET del Politecnico di Torino, Turin, Italy.
[iii] M.V. Lomonosov Moscow State University, D.V. Skobeltsyn Institute of Nuclear Physics, Moscow, Russia.
[iv] Department of Applied Physics, Aligarh Muslim University, Aligarh, India.
[v] Institute of Theoretical Physics, University of Wroclaw, Poland.